Transient effects in quantum dots contacted via topological superconductor

R. Taranko,[1] K. Wrześniewski,[2] I. Weymann,[2] and T. Domański[1]
[1]*Institute of Physics, Maria Curie-Skłodowska University, 20-031 Lublin, Poland*
[2]*Institute of Spintronics and Quantum Information, Faculty of Physics, Adam Mickiewicz University, 61-614 Poznań, Poland*

(Received 7 March 2024; revised 26 June 2024; accepted 28 June 2024; published 10 July 2024)

We investigate gradual development of the quasiparticle states in two quantum dots attached to opposite sides of the topological superconducting nanowire, hosting the boundary modes. Specifically, we explore the nonequilibrium cross-correlations transmitted between these quantum dots via the zero-energy Majorana modes. Our analytical and numerical results reveal the nonlocal features observable in the transient behavior of electron pairing, which subsequently cease while the hybrid structure evolves towards its asymptotic steady-state configuration. We estimate duration of these temporary phenomena. Using the nonperturbative scheme of the time-dependent numerical renormalization group technique we also analyze nonequilibrium signatures of the correlation effects competing with the proximity induced electron pairing. These dynamical processes could manifest themselves in braiding protocols imposed on the topological and/or conventional superconducting quantum bits, using superconducting hybrid nanostructures.

DOI: 10.1103/PhysRevB.110.035413

I. INTRODUCTION

Majorana quasiparticles localized at the edges of one-dimensional chains [1], propagating along the boundaries of two-dimensional topological superconductors [2] and confined on internal defects in p-wave bulk superconductors [3] have recently been the topic of intensive studies (see, e.g., Refs. [4–9] and references cited therein). Such research interests are motivated by the exotic character of Majorana modes and additionally stimulated by perspectives for constructing stable quantum bits (immune to external perturbations due to topological protection) and for performing quantum computations (by virtue of their non-Abelian character) [10]. Majorana quasiparticles, realized in various platforms, including the minimalistic Kitaev chain consisting of two and three coupled quantum dots [11,12], always emerge in pairs. To what extent, however, these spatially separated zero-energy modes are cross-correlated either statically (enabling teleportation phenomena [13–16]) or dynamically is still a matter of controversy. Some theoretical studies have predicted that Majorana modes might exhibit their dynamical interdependence in the shot-noise [17–20]. However, any evidence for such nonlocal cross-correlations is missing.

Another convenient platform for exploring the unique features of Majorana modes are hybrid structures, where single or multiple quantum dots are side-attached to topological superconductors [7]. The natural tendency of Majorana modes to be harbored at the outskirts of low-dimensional superconductors gives rise to their leakage onto the attached quantum dot(s) [21–25]. Such leakage has been indeed reported experimentally [26], stimulating further theoretical studies concerning the interplay of Majorana modes with the correlation-driven effects [27–38]. Here we propose to consider similar hybrid structures, comprising two quantum dots interconnected through the topological superconductor, in order to search for possible signatures of their nonlocal feedback effects appearing under nonequilibrium conditions.

Specifically, we investigate the dynamical properties of our setup (displayed in Fig. 1) right after coupling its constituents. The system consists of two quantum dots hybridized with the topological superconducting nanowire, hosting the Majorana boundary modes. One of the quantum dots, QD_1, is embedded between the conventional superconductor (S) and normal (N) leads, enabling its quasiparticles to be probed by the Andreev (electron-to-hole scattering) spectroscopy. The second quantum dot, QD_2, is flanked on the opposite side of the topological superconductor. These spatially distant quantum dots are communicated solely through the Majorana zero-energy modes of the topological superconductor. In what follows, we inspect nonlocal phenomena, appearing in the transient dynamics of measurable observables.

It is important to note that the time-resolved studies of topological superconductors have so far addressed various aspects, including their dynamics imposed by quantum quench across the topological transition in the Rashba nanowires [39,40], the nonequilibrium effects induced upon switching on and off the topological phase in segments of the Kitaev chains [41,42], gradual leakage of the Majorana mode onto single quantum dot [43], the crossed-Andreev and ballistic charge-transfer processes [15], nonequilibrium dynamics of the Majorana-Josephson system [44], as well as the waiting times of a topological Andreev interferometer [45]. As regards the nonlocal effects, they have been mainly investigated under the static conditions, considering finite hybridization of the Majorana modes [32]. Our study is therefore complementary to those, focusing on the nonlocal dynamical effects detectable in the hybrid structures with topological superconducting nanowire.

For microscopic considerations we assume the constituents of our setup to be disconnected until $t = 0$. After coupling them, we explore the quantum evolution of physical observables (for $t > 0$). In particular, we determine the charge occupancy of both quantum dots, the local and nonlocal

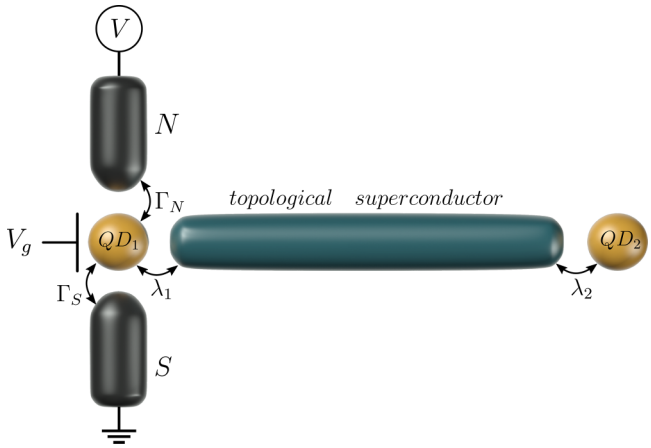

FIG. 1. Schematic view of two quantum dots attached to the opposite sides of the topological superconducting nanowire, hosting Majorana boundary modes. The first quantum dot, QD_1, is placed between the normal lead (N) and conventional superconductor (S), so that its emerging quasiparticles can be probed by the Andreev spectroscopy. The second quantum dot, QD_2, is floating.

electron pairings, and the charge current flowing through QD_1 in the unbiased and biased setup. The differential conductance of such current could enable empirical detection of the gradually emerging trivial and topological bound states of QD_1. We find that nonlocal effects extend solely over the transient region and later on (when additional abrupt or continuous changes are imposed on the energy levels of quantum dots and/or the coupling to external leads) they completely vanish.

This paper is organized as follows: In Sec. II we formulate the microscopic model. Section III presents the method relevant to uncorrelated system and discusses the analytical and numerical results obtained in the transient region of the unbiased setup. Next, in Sec. IV, we show the numerical results for the time-dependent charge transport induced by the voltage applied across QD_1 between the external N-S leads. In Sec. V we study the competition of the Coulomb repulsion with the superconducting proximity effect, manifested in the local and nonlocal electron pairings, by means of the time-dependent numerical renormalization group method. Section VI concludes the paper and summarizes the main findings. Appendixes A and B present useful technical details, concerning derivation of the time-dependent physical observables.

II. MICROSCOPIC MODEL

The hybrid structure displayed in Fig. 1 can be modeled by the following Hamiltonian:

$$\hat{H} = \sum_{i=1,2} \hat{H}_{QD_i} + \sum_{\beta=N,S} \left(\hat{H}_\beta + \hat{H}_{QD_1-\beta}\right) + \hat{H}_{M-DQD}. \quad (1)$$

The ith quantum dot (QD_i) is treated as the Anderson-type impurity

$$\hat{H}_{QD_i} = \sum_\sigma \varepsilon_i \hat{d}^\dagger_{i\sigma} \hat{d}_{i\sigma} + U \hat{n}_{i\uparrow} \hat{n}_{i\downarrow}, \quad (2)$$

where the operator $\hat{d}_{i\sigma}$ ($\hat{d}^\dagger_{i\sigma}$) annihilates (creates) electron with spin $\sigma = \uparrow, \downarrow$ at the energy level ε_i and U is the Coulomb repulsion between opposite-spin electrons.

We assume that QD_1 is embedded between the superconducting ($\beta = S$) and normal ($\beta = N$) leads. The superconductor is described by the BCS-type Hamiltonian $\hat{H}_S = \sum_{\mathbf{k},\sigma} \xi_{S\mathbf{k}} \hat{c}^\dagger_{S\mathbf{k}\sigma} \hat{c}_{S\mathbf{k}\sigma} - \sum_{\mathbf{k}} (\Delta_{SC} \hat{c}^\dagger_{S\mathbf{k}\uparrow} \hat{c}^\dagger_{S-\mathbf{k}\downarrow} + \text{H.c.})$, where the pairing gap Δ_{SC} is isotropic and the energies $\xi_{S\mathbf{k}} = \varepsilon_{S\mathbf{k}} - \mu_S$ are expressed with respect to the chemical potential μ_S. The normal lead is treated as a free fermion gas of itinerant electrons, $\hat{H}_N = \sum_{\mathbf{k},\sigma} \xi_{N\mathbf{k}} \hat{c}^\dagger_{N\mathbf{k}\sigma} \hat{c}_{N\mathbf{k}\sigma}$, where $\xi_{N\mathbf{k}} = \varepsilon_{N\mathbf{k}} - \mu_N$. Practically, the latter can be thought of as a metallic tip of the scanning tunneling microscope (STM). External voltage V applied across the leads detunes the chemical potentials, $\mu_N - \mu_S = eV$, inducing the charge current. Such processes arise from the hybridization terms

$$\hat{H}_{QD_1-\beta} = \sum_{\mathbf{k},\sigma} (V_{\beta\mathbf{k}}\, \hat{d}^\dagger_{1\sigma} \hat{c}_{\beta\mathbf{k}\sigma} + V^*_{\beta\mathbf{k}}\, \hat{c}^\dagger_{\beta\mathbf{k}\sigma} \hat{d}_{1\sigma}), \quad (3)$$

where $V_{\beta\mathbf{k}}$ denote the corresponding tunnel matrix elements. We restrict our considerations to the Andreev (electron-to-hole) scattering regime, which occurs for small voltages, $|eV| < \Delta_{SC}$. Under such circumstances one can use the wide-band limit approximation, introducing the constant couplings, $\Gamma_\beta = \pi \sum_{\mathbf{k}} |V_{\beta\mathbf{k}}|^2 \delta(\varepsilon - \varepsilon_{\beta\mathbf{k}})$.

Focusing our study on transient phenomena in the subgap regime, we treat the pairing gap Δ_{SC} as the largest energy scale. Superconducting proximity effect can be then modeled by $\hat{H}_S + \hat{H}_{QD_1-S} \approx \Gamma_S (\hat{d}^\dagger_{1\downarrow} \hat{d}^\dagger_{1\uparrow} + \hat{d}_{1\uparrow} \hat{d}_{1\downarrow})$, where Γ_S plays the role of the electron pairing induced at QD_1 [46].

The last term in (1) describes the Majorana modes of the topological superconducting nanowire [21,22,47]

$$\hat{H}_{M-DQD} = \lambda_1 (\hat{d}^\dagger_{1\uparrow} - \hat{d}_{1\uparrow}) \hat{\gamma}_1 + i\lambda_2 \hat{\gamma}_2 (\hat{d}^\dagger_{2\uparrow} + \hat{d}_{2\uparrow}) + i\varepsilon_M \hat{\gamma}_1 \hat{\gamma}_2, \quad (4)$$

where $\hat{\gamma}^\dagger_i = \hat{\gamma}_i$ are self-Hermitian Majorana operators. We assume that only the spin-$\uparrow$ electrons of the quantum dots are coupled to these Majorana boundary modes with the coupling strength λ_i. For nanowires shorter than the superconducting coherence length one should take into account an overlap ε_M between the Majorana modes. Here we restrict ourselves to sufficiently long nanowires, where such overlap is practically negligible, unless stated otherwise.

For convenience, we recast the self-Hermitian operators $\hat{\gamma}_i = \hat{\gamma}^\dagger_i$ by the operators $\hat{f}^{(\dagger)}_i$ defined through the Bogoliubov transformation

$$\hat{\gamma}_1 = \frac{1}{\sqrt{2}} (\hat{f}^\dagger + \hat{f}), \quad (5)$$

$$\hat{\gamma}_2 = \frac{i}{\sqrt{2}} (\hat{f}^\dagger - \hat{f}), \quad (6)$$

which obey the anticommutation relations $\{\hat{f}, \hat{f}^\dagger\} = 1$ of the conventional fermion fields.

III. DYNAMICS OF UNBIASED SETUP

Let us first study the time-dependent physical observables of our unbiased hybrid structure, neglecting the correlations,

$U = 0$. For this purpose we adapt the method introduced earlier in Refs. [43,48,49]. Specifically, we solve the Heisenberg equations of motion $i\hbar\partial_t\hat{O} = [\hat{O}, \hat{H}]$ for the localized $\hat{d}^{(\dagger)}_{i\sigma}(t)$ and itinerant $\hat{c}^{(\dagger)}_{\beta\mathbf{k}\sigma}(t)$ electrons.

We assume the components of our setup (Fig. 1) to be disconnected until $t \leqslant 0$. This implies that initial ($t = 0$) expectation values of the mixed operators vanish, i.e., $\langle \hat{d}^{(\dagger)}_{i\sigma}(0)\hat{d}_{j\neq i\sigma'}(0)\rangle = 0$ [50]. The system is next abruptly formed and we study its evolution for $t > 0$ solving the coupled differential equations of the second quantization operators. It is convenient to introduce the Laplace transforms $O(s) = \int_0^\infty e^{-st}\hat{O}(t)dt$ to account for the initial conditions of arbitrary physical observables. This approach is reliable for uncorrelated structures, $U = 0$, but it can be also generalized by incorporating the perturbative treatment of interactions. Finally, the time-dependent observables $O(t)$ can be determined from the inverse Laplace transforms $\mathcal{L}^{-1}\{O(s)\}(t)$.

In what follows, we assume the energy levels of both quantum dots to be equal, $\varepsilon_i = 0$, for which we derive analytical expressions of the Laplace transforms for $\hat{d}^{(\dagger)}_{i\sigma}(s)$ and $\hat{f}^{(\dagger)}(s)$. Their inverse Laplace transforms yield analytical expressions for the expectation values of various local and nonlocal observables that are of interest in this paper. We also note that in the absence of correlations on the quantum dots the operator $\hat{d}^{(\dagger)}_{2\downarrow}(s)$ decouples from the system dynamics, therefore, we do not consider it in Secs. III and IV.

A. Laplace-transformed equations of motion

Heisenberg equations of motion for the localized electrons $\hat{d}^{(\dagger)}_{1\sigma}$ mix them (via the hybridization $V_{\beta\mathbf{k}}$) with equations for the itinerant electrons $\hat{c}^{(\dagger)}_{\beta\mathbf{k}\sigma}$. Their detailed derivation has been previously discussed by us in Refs. [48,49], considering a single quantum dot conventional N-QD-S nanostructure. In the present case, however, we must additionally take into account the operators $\hat{f}^{(\dagger)}(s)$ originating from the coupling λ_1 [43] and indirectly also the operators $\hat{d}^{(\dagger)}_{2\uparrow}$ because of the coupling λ_2.

After some algebra, we find the following Laplace transforms (valid for $\varepsilon_i = 0$)

$$\hat{d}_{1\uparrow}(s) = \hat{d}^\dagger_{1\uparrow}(0)\frac{\lambda_1^2(s+\Gamma_N)^2}{H_3(s)} + \hat{d}_{1\uparrow}(0)\frac{(s+\Gamma_N)H_1(s)}{H_3(s)} - i\hat{d}^\dagger_{1\downarrow}(0)\frac{\Gamma_S H_1(s)}{H_3(s)} + i\hat{d}_{1\downarrow}(0)\frac{\Gamma_S\lambda_1^2(s+\Gamma_N)}{H_3(s)} - i[\hat{f}(0)+\hat{f}^\dagger(0)]\frac{\lambda_1(s+\Gamma_N)}{\sqrt{2}H_2(s)} + \sum_{\mathbf{k}} V_{\mathbf{k}}\hat{S}_{\mathbf{k}}(s), \tag{7}$$

$$\hat{d}_{2\uparrow}(s) = \hat{d}_{2\uparrow}(0)\frac{s^2+\lambda_2^2}{s(s^2+2\lambda_2^2)} - \hat{d}^\dagger_{2\uparrow}(0)\frac{\lambda_2^2}{s(s^2+2\lambda_2^2)} + i\big[\hat{f}(0)-\hat{f}^\dagger(0)\big]\frac{\lambda_2}{\sqrt{2}(s^2+2\lambda_2^2)}, \tag{8}$$

$$\hat{f}(s) = i\big[\hat{d}^\dagger_{1\uparrow}(0)-\hat{d}_{1\uparrow}(0)\big]\frac{\lambda_1(s+\Gamma_N)}{\sqrt{2}H_2(s)} - [\hat{d}^\dagger_{1\downarrow}(0)+\hat{d}_{1\downarrow}(0)]\frac{\lambda_1\Gamma_S}{\sqrt{2}H_2(s)} + i[\hat{d}^\dagger_{2\uparrow}(0)+\hat{d}_{2\uparrow}(0)]\frac{\lambda_2}{\sqrt{2}(s^2+2\lambda_2^2)} + \hat{f}(0)A(s) + \hat{f}^\dagger(0)B(s) + \frac{i\lambda_1}{\sqrt{2}s}\sum_{\mathbf{k}} V_{\mathbf{k}}[\hat{S}^\dagger_{\mathbf{k}}(s) - \hat{S}_{\mathbf{k}}(s)], \tag{9}$$

where

$$H_1(s) = s^3 + 2\Gamma_N s^2 + \big(\Gamma_N^2+\Gamma_S^2+\lambda_1^2\big)s + \lambda_1^2\Gamma_N, \tag{10}$$

$$H_2(s) = s^3 + 2\Gamma_N s^2 + \big(\Gamma_N^2+\Gamma_S^2+2\lambda_1^2\big)s + 2\lambda_1^2\Gamma_N, \tag{11}$$

$$H_3(s) = \big(s^2+2s\Gamma_N+\Gamma_N^2+\Gamma_S^2\big)H_2(s), \tag{12}$$

$$A(s) = \frac{s^2+\lambda_2^2}{s(s^2+2\lambda_2^2)} - \frac{\lambda_1^2(s+\Gamma_N)}{sH_2(s)}, \tag{13}$$

$$B(s) = \frac{s^2\big(\lambda_2^2-\lambda_1^2\big) + s\Gamma_N\big(2\lambda_2^2-\lambda_1^2\big) + \lambda_2^2\big(\Gamma_N^2+\Gamma_S^2\big)}{\big(s^2+2\lambda_1^2\big)H_2(s)}, \tag{14}$$

$$\hat{S}_{\mathbf{k}}(s) = \frac{\hat{c}^\dagger_{\mathbf{k}\downarrow}(0)H_1(s)\Gamma_S}{H_3(s)(s-i\xi_{\mathbf{k}})} - i\frac{\hat{c}_{\mathbf{k}\uparrow}(0)H_1(s)(s+\Gamma_N)}{H_3(s)(s+i\xi_{\mathbf{k}})} + \frac{\hat{c}_{\mathbf{k}\downarrow}(0)\lambda_1^2(s+\Gamma_N)\Gamma_S}{H_3(s)(s+i\xi_{\mathbf{k}})} + i\frac{\hat{c}^\dagger_{\mathbf{k}\uparrow}(0)\lambda_1^2(s+\Gamma_N)^2}{H_3(s)(s-i\xi_{\mathbf{k}})}, \tag{15}$$

where we now use $V_{\mathbf{k}} \equiv V_{N\mathbf{k}}$, $\hat{c}^\dagger_{\mathbf{k}\sigma} \equiv \hat{c}^\dagger_{N\mathbf{k}\sigma}$, $\xi_{\mathbf{k}} \equiv \xi_{N\mathbf{k}}$, and $\varepsilon_{\mathbf{k}} \equiv \varepsilon_{N\mathbf{k}}$. The Laplace transform of $\hat{d}_{1\downarrow}(s)$ can be obtained from the exact relation

$$\hat{d}_{1\downarrow}(s) = \frac{1}{s+\Gamma_N}\left[i\Gamma_S\hat{d}^\dagger_{1\uparrow}(s) + \hat{d}_{1\downarrow}(0) - i\sum_{\mathbf{k}}\frac{V_{\mathbf{k}}\hat{c}_{\mathbf{k}\downarrow}(0)}{s+i\xi_{\mathbf{k}}}\right]. \tag{16}$$

We can notice that $\hat{d}^{(\dagger)}_{1\sigma}(s)$ does not depend on the second quantum dot operators $\hat{d}^{(\dagger)}_{2\sigma'}(0)$. Similarly, the operator $\hat{d}^{(\dagger)}_{2\uparrow}(s)$ neither depends on $\hat{d}^{(\dagger)}_{1\sigma'}(0)$ nor on $\hat{c}^{(\dagger)}_{\mathbf{k}\sigma'}(0)$. Such properties are shown here explicitly for $\varepsilon_i = 0$, but they are valid for arbitrary energy levels as well. On this basis, one can expect that physical observables corresponding to different quantum dots should be independent of one another. For instance, the charge occupancy of QD_1 should neither depend on the coupling λ_2 nor the energy level ε_2. In other words, the charges accumulated at the quantum dots at a given time instant $t > 0$ are expected to be uncorrelated [51]. In the remaining part of this section we check whether such expectation is really true.

Using the inverse Laplace transforms of $\hat{d}^{(\dagger)}_{i\sigma}(s)$ we can explicitly determine the charge occupancy at each quantum dot $n_{i\sigma}(t) = \langle \hat{d}^\dagger_{i\sigma}(t)\hat{d}_{i\sigma}(t)\rangle$, the induced on-dot $\langle \hat{d}_{i\downarrow}(t)\hat{d}_{i\uparrow}(t)\rangle$, interdot $\langle \hat{d}_{1\downarrow}(t)\hat{d}_{2\uparrow}(t)\rangle$ electron pairings, etc. Another

quantity of our interest will be the charge current $j_{N\sigma}(t)$ flowing from the normal lead to QD_1 because (in presence of the external voltage $eV = \mu_N - \mu_S$) its differential conductance $G_\sigma(V,t) = \partial j_{N\sigma}(t)/\partial V$ could empirically probe the dynamically evolving quasiparticles of QD_1 (see Sec. IV).

For convenience, we assume the superconducting lead to be grounded, $\mu_S = 0$. To simplify notation, we set $\hbar = e = k_B = 1$ and use the coupling Γ_S as a unit for the energies, unless stated otherwise. In this convention, time will be expressed in units of $\hbar/\Gamma_S$ and the currents in units of $e\Gamma_S/\hbar$, respectively. In realistic situations $\Gamma_S \sim 200$ μeV, therefore typical timescales would of the order of ≈3.3 ps and the characteristic current unit would be ≈48 nA.

B. Time-dependent occupations

We start by investigating the time-dependent occupation number $n_{i\sigma}(t)$ of the quantum dots and another expectation value $n_f(t) = \langle \hat{f}^\dagger(t)\hat{f}(t)\rangle$, related with the Majorana quasiparticles. Below, we present explicit expression for the spin-↑ occupancy of QD_1 obtained for $\varepsilon_i = 0$ (its detailed derivation is presented in Appendix A). Using the Laplace transform (8), we find

$$n_{1\uparrow}(t) = M(t) + \sum_\sigma n_{1\sigma}(0) M_\sigma(t) + \frac{\Gamma_N}{\pi}\int_{-\infty}^{\infty} d\varepsilon \Phi_1(\varepsilon,t) - \frac{\Gamma_N}{\pi}\int_{-\infty}^{\infty} d\varepsilon f_N(\varepsilon)[\Phi_1(\varepsilon,t) - \Phi_2(\varepsilon,t)], \tag{17}$$

where

$$M_\uparrow(t) = \left(\mathcal{L}^{-1}\left\{\frac{(s+\Gamma_N)H_1(s)}{H_3(s)}\right\}(t)\right)^2 - \lambda_1^4\left(\mathcal{L}^{-1}\left\{\frac{(s+\Gamma_N)^2}{H_3(s)}\right\}(t)\right)^2, \tag{18}$$

$$M_\downarrow(t) = \Gamma_S^2\lambda_1^4\left(\mathcal{L}^{-1}\left\{\frac{(s+\Gamma_N)}{H_3(s)}\right\}(t)\right)^2 - \Gamma_S^2\left(\mathcal{L}^{-1}\left\{\frac{H_1(s)}{H_3(s)}\right\}(t)\right)^2, \tag{19}$$

$$M(t) = \Gamma_S^2\left(\mathcal{L}^{-1}\left\{\frac{H_1(s)}{H_3(s)}\right\}(t)\right)^2 + \lambda_1^4\left(\mathcal{L}^{-1}\left\{\frac{(s+\Gamma_N)^2}{H_3(s)}\right\}(t)\right)^2 + \frac{\lambda_1^2}{2}\left(\mathcal{L}^{-1}\left\{\frac{(s+\Gamma_N)}{H_2(s)}\right\}(t)\right)^2, \tag{20}$$

$$\Phi_1(\varepsilon,t) = \Gamma_S^2\left|\mathcal{L}^{-1}\left\{\frac{H_1(s)}{(s+i\varepsilon)H_3(s)}\right\}(t)\right|^2 + \lambda_1^4\left|\mathcal{L}^{-1}\left\{\frac{(s+\Gamma_N)^2}{(s+i\varepsilon)H_3(s)}\right\}(t)\right|^2, \tag{21}$$

$$\Phi_2(\varepsilon,t) = \left|\mathcal{L}^{-1}\left\{\frac{(s+\Gamma_N)H_1(s)}{(s+i\varepsilon)H_3(s)}\right\}(t)\right|^2 + \lambda_1^4\Gamma_S^2\left|\mathcal{L}^{-1}\left\{\frac{(s+\Gamma_N)}{(s-i\varepsilon)H_3(s)}\right\}(t)\right|^2, \tag{22}$$

and $f_N(\varepsilon) = [1+\exp(\varepsilon/T)]^{-1}$ is the Fermi-Dirac distribution function, with T being the temperature and $k_B \equiv 1$. In calculations we assume $T \to 0$. The opposite spin occupancy $n_{1\downarrow}(t)$ can be obtained in the same manner [see Eq. (A3) in Appendix A]. Analytical determination of $n_{1\downarrow}(t)$ is here feasible, because all needed inverse Laplace transforms $\mathcal{L}^{-1}\{F(s)\}(t)$ can be represented in a fractional form $F(s) = (s-s_1)\cdots(s-s_n)/(s-s_{n+1})\cdots(s-s_m)$, where $2n < m$.

In agreement with the expectations, we notice that $n_{1\uparrow}(t)$ is independent of the initial fillings of $n_{2\sigma}(0)$ and $n_f(0)$. The term $M(t)$ [see the last part of Eq. (20)], however, contributes some influence of the Majorana modes to $n_{1\uparrow}(t)$ because $\hat{d}_{1\uparrow}(t)$ expanded in terms of the electron operators at $t = 0$ contains nonvanishing contribution proportional to $\hat{f}(0)$ and $\hat{f}^\dagger(0)$

$$-i[\hat{f}(0) + \hat{f}^\dagger(0)]\frac{\lambda_1}{\sqrt{2}}\mathcal{L}^{-1}\left\{\frac{s+\Gamma_N}{H_2(s)}\right\}(t). \tag{23}$$

For $\Gamma_N = 0$, this expression yields

$$\frac{\lambda_1^2}{2}\frac{\sin\left(t\sqrt{\Gamma_S^2+2\lambda_1^2}\right)}{\Gamma_S^2+2\lambda_1^2}. \tag{24}$$

Such a term does not depend on $n_f(0)$, but it reveals the influence of QD_1 coupling λ_1 to the topological nanowire.

The parts which depend on the initial occupancy of QD_1 are separated from another contribution dependent on the itinerant electrons of the normal lead, represented by the last terms of Eq. (17). Notice, however, that some information about coupling with the normal lead enters M, $M_\uparrow$, and $M_\downarrow$ through the term with Γ_N. It is interesting that $n_{1\sigma}(t)$ is independent of any parameter characterizing QD_2 [i.e. λ_2, $\varepsilon_{2\uparrow}$, $n_{2\sigma}(0)$]. Such dependence could eventually arise only for nonvanishing overlap $\varepsilon_M \neq 0$ between the Majorana modes.

Let us now analyze in some detail the case $\Gamma_N = 0$, for which explicit expressions can be derived. Assuming the initial empty fillings of both QDs, $n_{i\sigma}(0) = 0$, from the general expression (17) we obtain

$$n_{1\uparrow}(t) = \frac{1}{2} + \frac{\Gamma_S}{2\sqrt{\Gamma_S^2+2\lambda_1^2}}\sin(t\Gamma_S)\sin\left(t\sqrt{\Gamma_S^2+2\lambda_1^2}\right) - \frac{1}{2}\cos(t\Gamma_S)\cos\left(t\sqrt{\Gamma_S^2+2\lambda_1^2}\right), \tag{25}$$

$$n_{1\downarrow}(t) = \frac{1}{2} + \frac{\Gamma_S}{2\sqrt{\Gamma_S^2+2\lambda_1^2}}\sin(t\Gamma_S)\sin\left(t\sqrt{\Gamma_S^2+2\lambda_1^2}\right) - \frac{\Gamma_S^2}{2\left(\Gamma_S^2+2\lambda_1^2\right)}\cos(t\Gamma_S)\cos\left(t\sqrt{\Gamma_S^2+2\lambda_1^2}\right) - \frac{\lambda_1^2}{\Gamma_S^2+2\lambda_1^2}\cos(t\Gamma_S). \tag{26}$$

For vanishing λ_1 the occupancy has an oscillatory behavior

$$n_{1\sigma}(t) = \sin^2(t\Gamma_S), \tag{27}$$

with the time period equal to π/Γ_S. For the opposite case $\lambda_1 \gg \Gamma_S$, we can rewrite Eqs. (25) and (26) in the following

approximate forms:

$$n_{1\uparrow}(t) \simeq \tfrac{1}{2}[1 - \cos(t\Gamma_S)\cos(\sqrt{2}t\lambda_1)], \tag{28}$$

$$n_{1\downarrow}(t) \simeq \sin^2\left(\frac{t\Gamma_S}{2}\right). \tag{29}$$

The occupancy of QD_2 behaves quite differently in comparison to $n_{1\sigma}(t)$. From Eq. (8) we can notice that the operator $\hat{d}_{2\uparrow}(s)$ is not coupled to a continuous spectrum of the normal lead, i.e., it does not depend on Γ_N. For this reason we get its undamped oscillations. Assuming the initial condition $n_{2\uparrow}(0) = 0$, we analytically obtain

$$n_{2\uparrow}(t) = \frac{2\lambda_2^2}{2\lambda_2^2 + \varepsilon_2^2} \sin^2\left(\frac{t}{2}\sqrt{2\lambda_2^2 + \varepsilon_2^2}\right), \tag{30}$$

with the period $2\pi/(2\lambda_2^2 + \varepsilon_2^2)^{1/2}$ and the constant amplitude (unaffected by the coupling of QD_1 to the normal lead). Only for a finite overlap between the Majorana modes, $\varepsilon_M \neq 0$, the relaxation processes could be activated, driving the occupancy of QD_2 towards its steady limit ($t \to \infty$) value.

Using Eq. (9) for $\hat{f}(s)$, we can determine the time-dependent occupancy $n_f(t)$. For $\varepsilon_i = 0$ and $\Gamma_N = 0$, it is given by

$$n_f(t) = \frac{1}{2} + [2n_f(0) - 1]\cos(\sqrt{2}\lambda_2 t) \times \left[\frac{\lambda_1^2}{\Gamma_S^2 + 2\lambda_1^2}\cos\left(t\sqrt{\Gamma_S^2 + 2\lambda_1^2}\right) + \frac{\Gamma_S^2}{2\left(\Gamma_S^2 + 2\lambda_1^2\right)}\right], \tag{31}$$

which turns out to be independent of the initial values of $n_{i\sigma}(0)$.

Figure 2 presents the time-dependent occupancies computed numerically for $\lambda_1 = \lambda_2 = 8$, assuming $\Gamma_N = 0$ [Fig. 2(a)] and $\Gamma_N \neq 0$ [Fig. 2(b)]. We note that the obtained results nearly coincide with the approximate formulas (28) and (29). The spin-$\downarrow$ occupancy of QD_1 has a similar form as for the $\lambda_1 = 0$ case, but the oscillations are twice slower with the period equal to $2\pi/\Gamma_S$. Note that, generally, the oscillations of $n_{1\sigma}(t)$ are substantially different for each spin component. In the time-dependent occupancy $n_{1\uparrow}(t)$ we observe superposition of two oscillations: the fast ones, with the period equal to $\sqrt{2}\pi/\lambda_1$, and the amplitude oscillations, with the time period equal to $2\pi/\Gamma_S$ (related to the proximitized QD_1 in absence of the Majorana modes). On the other hand, the opposite spin occupancy $n_{1\downarrow}(t)$ oscillates with the period equal approximately to $2\pi/\Gamma_S$, cf. Eq. (29).

Let us now analyze the occupation dynamics in the case of finite coupling Γ_N. The corresponding results are shown in Fig. 2(b), while in Fig. 3 we present detailed behavior of $n_{1\sigma}(t)$ together with contributions stemming from relevant terms of the analytical formulas. First of all, one can note that now a damping of the oscillatory behavior occurs, see Fig. 2(b). This is even more revealed in different contributions to $n_{1\sigma}(t)$. In particular, the dashed-green line represents the contribution from the term $M(t)$, cf. Eq. (20). One can clearly observe its damped oscillations caused by the coupling Γ_N. On the other hand, the black-dashed line represents the contribution due to the coupling of QD_1 to a continuous spectrum of the normal lead, which basically describes the envelope of the oscillations. The total sum of these contributions gives the resulting time-dependent occupancy $n_{1\uparrow}(t)$ displayed by the red curve in Fig. 3. The stationary limit value $n_{1\uparrow}(t \to \infty) = 0.5$ is approached after a sequence of quantum oscillations with the exponentially suppressed amplitude. Performing similar calculations for $n_{1\downarrow}(t)$ we get the result presented by the thick solid line. Now, the fast oscillations are very much suppressed and one only observes slow oscillations decaying towards the steady-state value of $1/2$, see the blue curve in Fig. 3.

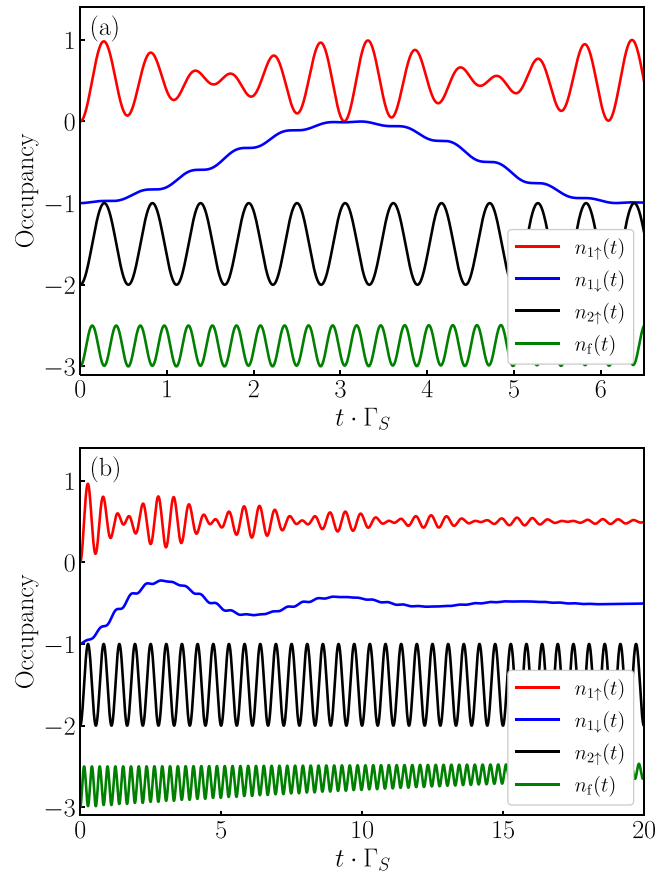

FIG. 2. Time-dependent occupancies $n_{i\sigma}(t)$ of both quantum dots (as indicated) and $n_f(t)$ for $\lambda_1 = \lambda_2 = 8$, $\varepsilon_1 = \varepsilon_2 = 0$, assuming the initial conditions $n_{i\sigma}(0) = n_f(0) = 0$, and $\Gamma_N = 0$ (upper panel), $\Gamma_N = 0.2$ (bottom panel). For clarity the curves are vertically shifted by one (their initial value is zero). All parameters are expressed in units of $\Gamma_S \equiv 1$.

C. Time dependence of the on-dot pairing

The time-dependent electron populations of the individual quantum dots are further interrelated with development of the local and nonlocal pairings. Let us study this issue, first considering the singlet pairing

$$C_{11}(t) \equiv \langle \hat{d}_{1\downarrow}(t)\hat{d}_{1\uparrow}(t)\rangle \tag{32}$$

induced on QD_1 via its proximity to the (trivial) bulk superconductor. We can analytically determine $C_{11}(t)$ using the inverse Laplace transforms of the operators $\hat{d}_{1\sigma}(s)$ and following the procedure, which is analogous to the calculations of

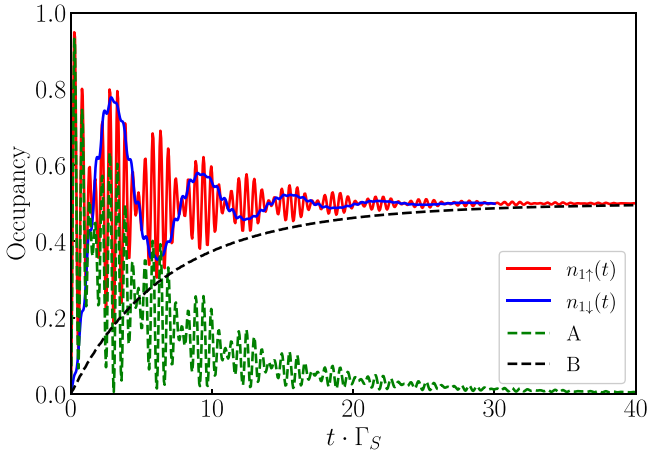

FIG. 3. The time-dependent occupancies $n_{1\sigma}(t)$ obtained for the same set of model parameters as in Fig. 2 with $\Gamma_N = 0.2$. To clarify the behavior of $n_{1\uparrow}(t)$ we show the contributions from the term $M(t)$ (curve *A*) and the last term of Eq. (7) (curve B).

the charge occupancy $n_{1\sigma}(t)$. For the initially empty quantum dots and $\varepsilon_i = 0$, the on-dot pairing (32) is given by

$$C_{11}(t) = D(t) + i\Gamma_N\Gamma_S \int_{-\infty}^{\infty} \frac{d\varepsilon}{\pi}[f_N(\varepsilon)D_1(\varepsilon,t) + D_2(\varepsilon,t)], \tag{33}$$

with functions $D(t)$ and $D_{1,2}(\varepsilon,t)$ presented explicitly by Eqs. (A10)–(A12) in Appendix A.

We notice the absence of any term dependent on λ_2. It means that electron pairing induced at QD_1 is completely unaffected by the second QD_2. The pairing function (33) depends on the initial filling of QD_1, whereas it has no dependence on $n_f(0)$, despite the appearance of operators $\hat{f}(0)$ and $\hat{f}^\dagger(0)$ in the Laplace transform of $\hat{d}_{1\uparrow}(s)$. Such terms yield the following result [see the last part of Eq. (A10)]

$$\langle[\hat{f}(0) + \hat{f}^\dagger(0)]^2\rangle \frac{i\Gamma_S\lambda_1^2}{2}\mathcal{L}^{-1}\left\{\frac{1}{H_2(s)}\right\}(t)\mathcal{L}^{-1}\left\{\frac{s+\Gamma_N}{H_2(s)}\right\}(t), \tag{34}$$

which is indeed independent of $n_f(0)$.

For $\Gamma_N = 0$ and initially empty QD_1, the pairing correlation function $C_{11}(t)$ is purely imaginary. It can be written in the following simple form:

$$C_{11}(t) = -\frac{i}{2}\Bigg[\frac{\lambda_1^2}{\Gamma_S^2+2\lambda_1^2}\sin(t\Gamma_S) + \frac{\Gamma_S^2+\lambda_1^2}{\Gamma_S^2+2\lambda_1^2} \times \sin(t\Gamma_S)\cos\left(t\sqrt{\Gamma_S^2+2\lambda_1^2}\right) + \frac{\Gamma_S}{\sqrt{\Gamma_S^2+2\lambda_1^2}} \times \cos(t\Gamma_S)\sin\left(t\sqrt{\Gamma_S^2+2\lambda_1^2}\right)\Bigg], \tag{35}$$

representing a combination of the oscillations with frequencies Γ_S and $(\Gamma_S^2+2\lambda_1^2)^{1/2}$, respectively. For $\lambda_1 \gg \Gamma_S$, the oscillations are characterized by a small period $\approx 2\pi/(\Gamma_S^2+2\lambda_1^2)^{1/2}$ and the amplitude modulated by another periodicity of $2\pi/\Gamma_S$. In this case $C_{11}(t) \approx -\frac{i}{2}\sin(t\Gamma_S)\cos^2[\frac{t}{2}(\Gamma_S^2+2\lambda_1^2)^{1/2}]$.

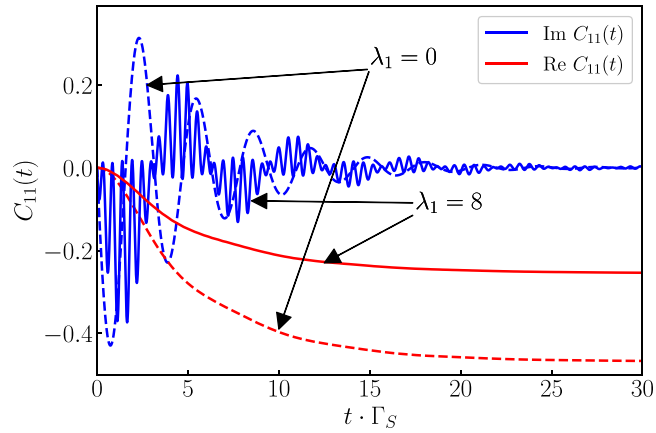

FIG. 4. The on-dot pairing $C_{11}(t)$ induced at QD_1 obtained for the same set of model parameters as in the bottom panel of Fig. 2 with $\lambda_1 = 8$ (solid lines). For comparison, we also show $C_{11}(t)$ in the absence of topological nanowire, i.e., for $\lambda_1 = 0$ (dashed curves).

For small values of the coupling λ_1, one can neglect the terms proportional (and of higher order) to $(\frac{\lambda_1}{\Gamma_S})^2$ and get $C_{11}(t) \approx -\frac{i}{2}\sin(2t\Gamma_S)$. This result is identical to the case when QD_1 is coupled only to the superconducting lead, cf. Refs. [48,49]. For $\Gamma_N \neq 0$, the on-dot pairing becomes a complex function. Its real part originates from the last term in Eq. (8) stemming from continuous spectrum of the normal lead. This part depends on the Fermi level of the normal lead, see Eq. (A3).

Figure 4 displays the time-dependent pairing $C_{11}(t)$ obtained for the unbiased setup ($\mu = 0$) and for finite Γ_N. We observe an oscillating structure of the imaginary part, similar to the behavior of $n_{1\uparrow}(t)$, cf. Figs. 2 and 3. This is related to the transient charge current, flowing through QD_1. These oscillations are damped, because of a continuum states responsible for the relaxation processes at QD_1. On the other hand, the real part evolves monotonically to its asymptotic (negative) value. For comparison, we also plot the complex function $C_{11}(t)$ for the case of $\lambda_1 = 0$, i.e. when QD_1 is embedded only between the normal and superconducting leads [49]. The structure of $\mathrm{Im}C_{11}(t)$ manifests the high-frequency oscillations $\approx(\Gamma_S^2+2\lambda_1^2)^{1/2}$ coexisting with the beats of frequency $\approx\Gamma_S$. Note that for vanishing λ_1 the imaginary part of $C_{11}(t)$ exhibits only one component oscillations with the frequency equal to Γ_S.

For hybrid structures, where topological superconductivity is induced by contacting the semiconducting nanowires with bulk superconductors, one has to take into consideration the influence of external magnetic field responsible for the Zeeman splitting of the quantum dot energy levels, $B_z = \varepsilon_{i\downarrow} - \varepsilon_{i\uparrow}$. In analogy to a detrimental role of magnetic impurities in bulk superconductors, this Zeeman splitting turns out to suppress the electron pairing at QD_1 (see Fig. 5). One can notice that the magnitude of the stationary on-dot pairing $|C_{11}(t \to \infty)|$ gets reduced upon increasing the magnetic field. Furthermore, the transient region narrows and the oscillations of the complex function $C_{11}(t)$ acquire rather complicated profiles, due to transitions between the Majorana zero-energy mode and the spin-polarized Andreev states.

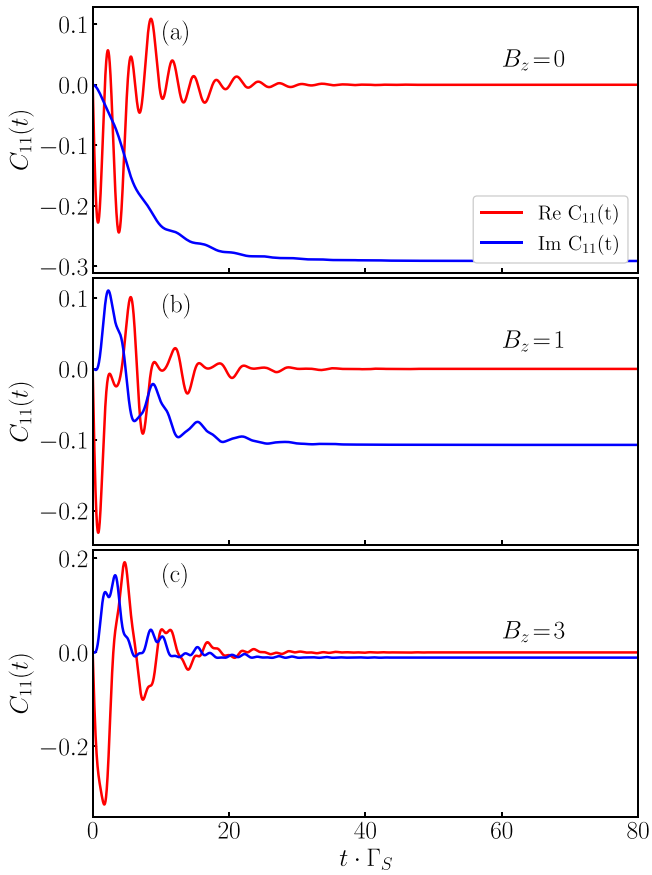

FIG. 5. Transient dynamics of the on-dot pairing $C_{11}(t)$ obtained for different values of the magnetic field $B_z = 0$, 1, and 3, using the same set of model parameters as in Fig. 2.

D. Time-dependent interdot pairing

We now consider the nonlocal electron pairing induced between the spatially distant quantum dots. In analogy to the previous section, we focus on the singlet pairing

$$C_{12}(t) \equiv \langle \hat{d}_{1\downarrow}(t)\hat{d}_{2\uparrow}(t)\rangle. \tag{36}$$

In practice this sort of electron pairing could be detected via the crossed Andreev reflections in hybrid structures with an additional electrode contacted to QD_2. Let us remark that $C_{12}(t)$ originates from the local pairing of QD_1 electrons, which is further extended onto QD_2 by the Majorana quasiparticles. Technically this is provided by the operators $\hat{f}^{(\dagger)}(0)$ appearing in the Laplace transforms of $\hat{d}_{1\downarrow}(s)$ and $\hat{d}_{2\uparrow}(s)$ [see Eqs. (8) and (16)]. For $\varepsilon_i = 0$ we find

$$C_{12}(t) = i\lambda_1\lambda_2\Gamma_S\left[\frac{1}{2} - n_f(0)\right] \times \mathcal{L}^{-1}\left\{\frac{1}{H_2(s)}\right\}(t)\mathcal{L}^{-1}\left\{\frac{1}{s^2+2\lambda_2^2}\right\}(t). \tag{37}$$

In the limit of $\Gamma_N = 0$ the pairing $C_{12}(t)$ simplifies to

$$C_{12}(t) = \frac{i\lambda_1\Gamma_S}{\sqrt{2}\left(\Gamma_S^2+2\lambda_1^2\right)}[1-2n_f(0)] \times \sin\left(\sqrt{2}t\lambda_2\right)\sin^2\left(\frac{t}{2}\sqrt{\Gamma_S^2+2\lambda_1^2}\right). \tag{38}$$

On the other hand, for finite Γ_N, we obtain

$$C_{12}(t) = \frac{i\lambda_1\Gamma_S}{2\sqrt{2}}[1-2n_f(0)]\sin\left(\sqrt{2}t\lambda_2\right) \times \frac{e^{-at}+e^{-bt}\left[\frac{a-b}{c}\sin(ct)-\cos(ct)\right]}{(b-a)^2+c^2}, \tag{39}$$

where the parameters a, b, c correspond to three roots s_i ($i = 1, 2, 3$) of the cubic equation $H_2(s_i) = 0$. One of these roots, say s_1, is real and it defines the positive-valued parameter $a > 0$ via $s_1 = -a$. The other parameters, b and c, are related with the conjugated roots $s_2 = s_3^\star$. They are expressed as $s_2 = -b + ic$ and $s_3 = -b - ic$, where $b > 0$.

Equation (39) implies that the interdot pairing (36) does not depend on the initial occupation $n_{i\sigma}(0)$ of the quantum dots. Furthermore, $C_{12}(t)$ has no explicit dependence on the voltage μ applied across QD_1 between the external leads because the operators $\hat{c}_{\mathbf{k}\sigma}(0)$ do not appear simultaneously in $\hat{d}_{1\downarrow}(t)$ and $\hat{d}_{2\uparrow}(t)$. Influence of the normal lead, however, enters indirectly through the roots s_1–s_3 (where a, b, and c depend on Γ_N). We observe that for $\Gamma_N = 0$ the amplitude of $C_{12}(t)$ oscillations diminishes upon increasing λ_1, whereas for $\Gamma_N \neq 0$, we observe a similar behavior, although with damped oscillations.

In general, the nonlocal pairing (36) is sensitive to the position of the energy levels ε_i of the quantum dots. It is purely imaginary only for $\varepsilon_2 = 0$. Otherwise, for $\varepsilon_2 \neq 0$ and arbitrary QD_1 energy level, the function $C_{12}(t)$ becomes complex with nonvanishing real and imaginary parts.

The time-dependent interdot pairing for selected values of the quantum dot energy levels is shown in Fig. 6. First of all, we notice that the interdot pairing survives only in the transient region. The time-dependent profile of this complex pairing function $C_{12}(t)$ is sensitive to specific values of the quantum dot energy levels. Additional effects can arise from the quantum quenches. The middle plot of Fig. 6 displays the evolution of $C_{12}(t)$ after a sudden change of ε_1 imposed at $t = 5/\Gamma_S$. This quench substantially affects the real and imaginary parts of the nonlocal pairing $C_{12}(t)$. It is evident that for $t \geqslant 5/\Gamma_S$ the time-dependent interdot pairing presented in the middle panel of Fig. 6 differs from the bottom panel, even though the energy levels are identical. We have checked, however, that signatures of the nonlocal pairing are completely absent in all quantum quenches imposed outside the transient regime. This observation emphasizes the subtle importance of transient phenomena, which enable mutual correlations between spatially distant quantum dots. Such dynamical nonlocal effects would be observable in the crossed Andreev transmission, and could possibly arise via the single-particle teleportation as well.

Let us also inspect the influence of the Zeeman field B_z on the nonlocal pairing $C_{12}(t)$ between opposite spin electrons (see Fig. 7). In analogy to $C_{11}(t)$, we notice that the magnetic field quickly suppresses this interdot pairing. Such effects are visible only in the transient region (because the stationary limit value of $C_{12}(t \to \infty)$ vanishes for all cases). This suppression arises from a competition of the magnetic field with the singlet pairing, no matter whether it is local or nonlocal.

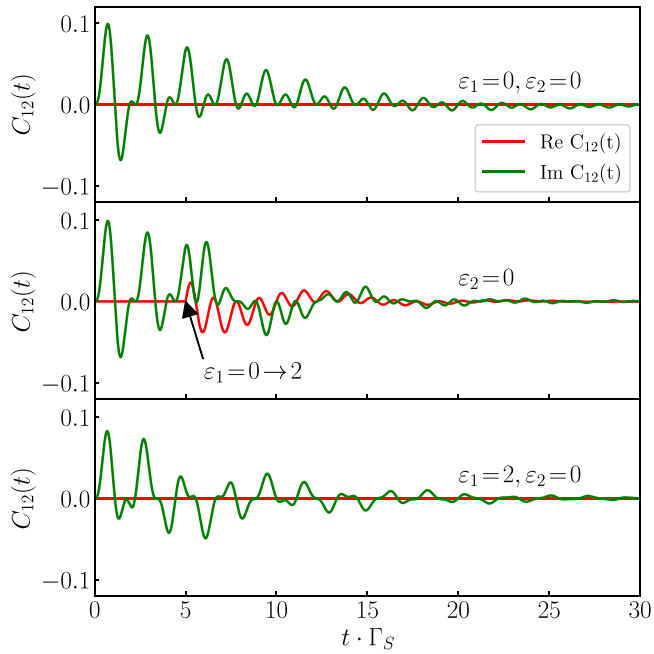

FIG. 6. The complex interdot pairing function $C_{12}(t)$ obtained for $\lambda_1=\lambda_2=2$, $\Gamma_N=0.2$ and several values of quantum dot energy levels, as indicated. The red curves refer to the real and the green curves to the imaginary parts of $C_{12}(t)$, respectively. The middle plot presents the evolution of $C_{12}(t)$ when imposing a sudden change of the energy level from $\varepsilon_1=0$ to $\varepsilon_1=2$ at $t=5/\Gamma_S$.

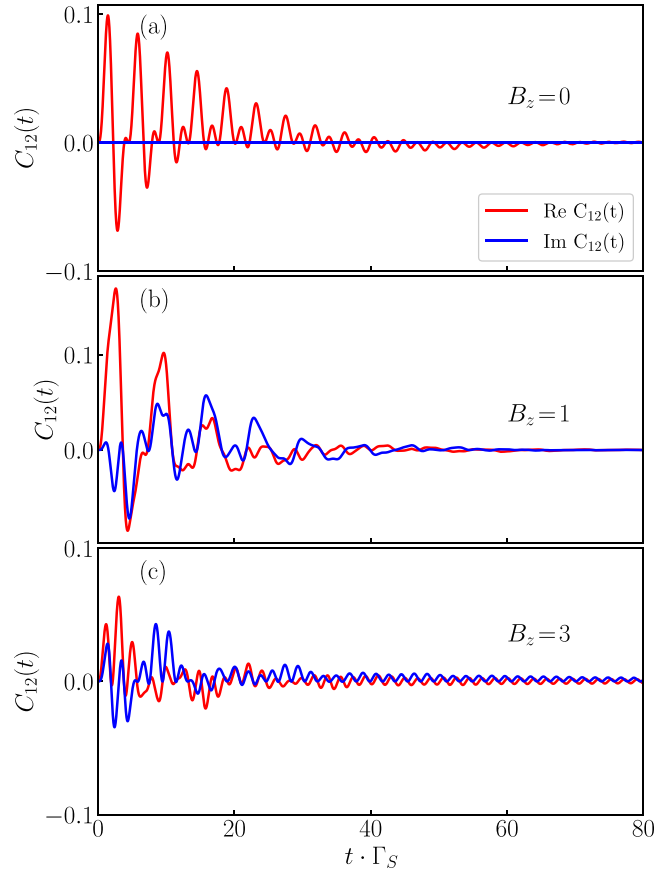

FIG. 7. Transient dynamics of the nonlocal pairing $C_{12}(t)$ in the singlet channel obtained for the same set of model parameters as in Fig. 5.

E. Dynamics of the triplet pairing

Finally let us consider the mixed pairing between QD_2 and the topological superconducting nanowire

$$C_{2f}(t)=\langle \hat{d}_{2\uparrow}(t)\hat{f}(t)\rangle. \tag{40}$$

This triplet pairing is associated with leakage of the Majorana mode onto the side-attached QD_2, and similar process occurs on QD_1 regardless of $n_{1\sigma}(0)$. Let us recall that from both operators $\hat{d}_{2\uparrow}(s)$ and $\hat{f}(s)$ only the latter depends on $\hat{c}^{(\dagger)}_{\mathbf{k}\sigma}(0)$. For this reason the mixed pairing (40) does not depend on the normal lead electrons and thereby on the bias voltage V.

In what follows, we focus on the initially empty dot $n_{2\uparrow}(0)=0$ and $n_f(0)=0$, assuming the isotropic couplings $\lambda_1=\lambda_2\equiv\lambda$. Under such conditions we obtain (for $\varepsilon_i=0$)

$$C_{2f}(t)=\frac{i}{2}\sin(\sqrt{2}\lambda t)\left[\cos^2\left(\frac{\lambda t}{\sqrt{2}}\right)+\lambda^2\mathcal{L}^{-1}\left\{\frac{s\Gamma_N+\Gamma_S^2+\Gamma_N^2}{(s^2+2\lambda^2)H_2(s)}\right\}(t)\right]. \tag{41}$$

For $\Gamma_N=0$, formula (41) simplifies to

$$C_{2f}(t)=\frac{i\sin(\sqrt{2}\lambda t)}{2\left(\Gamma_S^2+2\lambda^2\right)}\left[\Gamma_S^2+2\lambda^2\cos^2\left(\frac{\sqrt{\Gamma_S^2+2\lambda^2}}{2}t\right)\right], \tag{42}$$

revealing an oscillatory behavior. This analytical result (42) is valid when the quantum dots interconnected through the Majorana quasiparticles are not coupled to a continuous spectrum of the normal lead that could activate the relaxation processes. It appears, however, that even in the case of $\Gamma_N\neq 0$, the mixed pairing function (41) oscillates against time with nonvanishing amplitude. To observe it, we evaluated the pairing function (41) in the long-time limit

$$C_{2f}(t)=\frac{i}{2}\sin(\sqrt{2}\lambda t)\times\left[\cos^2\left(\frac{\lambda t}{\sqrt{2}}\right)2\lambda^2\Gamma_N\mathrm{Re}\left(\frac{e^{i\sqrt{2}\lambda t}s_{16}}{s_{12}s_{13}s_{14}s_{15}}\right)\right]. \tag{43}$$

Here $s_{nm}=s_n-s_m$, and $s_1=i\sqrt{2}\lambda$, $s_2=-s_1$, $s_3=-a$, $s_4=-b+ic$, $s_5=-b-ic$, $s_6=-(\Gamma_S^2+\Gamma_N^2)/\Gamma_N$, where s_3, s_4, s_5 are the roots of the cubic equation $H_2(s_i)=0$ and a, b are real positive parameters. In the large-t limit this pairing function is purely imaginary and it has oscillating character. The formula presented in Eq. (43) is valid for $\varepsilon_1=\varepsilon_2=0$. Otherwise, the operators $\hat{d}_{2\uparrow}(s)$ and $\hat{f}(s)$ depend on the energy levels ε_i affecting the pairing function $C_{2f}(t)$. In particular, the influence of QD_1 on the triplet pairing $C_{2f}(t)$ is incorporated via the operator $\hat{f}(s)$.

IV. TUNNELING CONDUCTANCE

In this section we study the differential conductance $G_\sigma(V,t)=\frac{\partial}{\partial V}j_{N\sigma}(t)$ of the time-dependent current $j_{N\sigma}(t)$, flowing between QD_1 and the normal lead. For convenience we express $G_\sigma(V,t)$ in units of $2e^2/h$ and investigate its dependence on the applied bias voltage V. We recall that $eV=\mu_N-\mu_S$ and the topological superconductor is assumed to be grounded $\mu_S=0$, such that $eV=\mu_N\equiv\mu$. The tunneling current can be determined from the evolution of the total number of electrons in the normal electrode. For our setup it can be written as [49]

$$j_{N\sigma}(V,t)=2\mathrm{Im}\sum_{\mathbf{k}}V_{\mathbf{k}}e^{-i\varepsilon_{\mathbf{k}}t}\langle\hat{d}^\dagger_{1\sigma}(t)\hat{c}_{\mathbf{k}\sigma}(0)\rangle-2\Gamma_N n_{1\sigma}(t). \tag{44}$$

Substituting the inverse Laplace transform of $\hat{d}_{1\uparrow}(s)$ [see Eq. (8)], we obtain the derivative of the first term appearing in Eq. (44) with respect to μ in the following way:

$$\begin{aligned}
&\frac{\partial}{\partial\mu}2\mathrm{Im}\left(i\sum_{\mathbf{k},\mathbf{k}_1}V_{\mathbf{k}}V_{\mathbf{k}_1}e^{-i\varepsilon_{\mathbf{k}}t}\mathcal{L}^{-1}\left\{\frac{(s+\Gamma_N)H_1(s)}{(s-\varepsilon_{\mathbf{k}_1})H_3(s)}\right\}(t)\langle\hat{c}^\dagger_{\mathbf{k}_1\uparrow}(t)\hat{c}_{\mathbf{k}\uparrow}(0)\rangle\right)\\
&=\frac{\partial}{\partial\mu}\frac{2\Gamma_N}{\pi}\mathrm{Re}\int_{-\infty}^{\infty}d\varepsilon f_N(\varepsilon)e^{-i\varepsilon t}\mathcal{L}^{-1}\left\{\frac{(s+\Gamma_N)H_1(s)}{(s-\varepsilon)H_3(s)}\right\}(t)\\
&=\frac{2\Gamma_N}{\pi}\mathrm{Re}\left(e^{-i\mu t}\mathcal{L}^{-1}\left\{\frac{(s+\Gamma_N)H_1(s)}{(s-\mu)H_3(s)}\right\}(t)\right).
\end{aligned}\tag{45}$$

In the next step we subsequently calculate $\partial n_{1\uparrow}(t)/\partial\mu$ taking into consideration only such terms which depend on the bias voltage [see Eq. (A2)]. As a result we get

$$\begin{aligned}
\frac{\partial n_{1\uparrow}(t)}{\partial\mu}=\frac{\Gamma_N}{\pi}\Bigg\{&\Gamma_S^2\lambda_1^4\left|\mathcal{L}^{-1}\left\{\frac{s+\Gamma_N}{(s+i\mu)H_3(s)}\right\}(t)\right|^2+\left|\mathcal{L}^{-1}\left\{\frac{(s+\Gamma_N)H_1(s)}{(s+i\mu)H_3(s)}\right\}(t)\right|^2\\
&-\Gamma_S^2\left|\mathcal{L}^{-1}\left\{\frac{H_1(s)}{(s+i\mu)H_3(s)}\right\}(t)\right|^2-\lambda_1^4\left|\mathcal{L}^{-1}\left\{\frac{(s+\Gamma_N)^2}{(s+i\mu)H_3(s)}\right\}(t)\right|^2\Bigg\}.
\end{aligned}\tag{46}$$

The definition $G_\uparrow(V,t)=\frac{\partial}{\partial V}j_{N\uparrow}(V,t)$ along with Eqs. (44), (45), and (46) yield the information on time-dependent quasiparticle states of our hybrid structure. The relevant inverse Laplace transforms can be obtained in a form of the linear combinations of $\exp(-\Gamma_N t)$ and $\exp(-s_i t)$ with coefficients being the functions of $s_1,\ldots,s_8$, where $s_1=-\Gamma_N+i\Gamma_S$, $s_2=-\Gamma_N-i\Gamma_S$ and s_3, s_4, s_5 (s_6, s_7, s_8) are solutions of the cubic equation $H_1(s)=0$ [$H_2(s)=0$].

Figure 8 presents the time-dependent conductance versus the bias voltage V obtained for $\lambda=0.6$, 1, and 2 ($\lambda\equiv\lambda_1=\lambda_2$), respectively. It shows how the quasiparticle peaks of QD_1 develop in time. For weak couplings, $\lambda=0.6$ and 1, we observe roughly two quasiparticle peaks emerging from the initial broad structure, see Figs. 8(a) and 8(b). Their steady-limit shape establishes at relatively long time in comparison with the results obtained for a stronger coupling, $\lambda=2$. After a closer inspection, however, we can notice some tiny splitting between the maxima. In contrast, for larger coupling λ, there appear four quasiparticle peaks well separated from one another. Their steady limit structure establishes pretty fast, nearly at $t\approx 5/\Gamma_S$. The duration of the transient region is thus strongly sensitive to the coupling strength λ.

In Fig. 9 we present the steady limit differential conductance $G_\sigma(V,t\to\infty)$ obtained for different couplings λ, as indicated. Since one of the solutions, s_3 (s_6) for the cubic equation has a negative real value and the other solutions are complex (with negative real parts), we get

$$\begin{aligned}
G_\uparrow(\mu,\infty)=2\Gamma_N\mathrm{Re}\left(\frac{\phi_1(\mu)}{\phi_3(\mu)}\right)-2\Gamma_N^2\big[|\phi_1(\mu)|^2-\Gamma_S^2|\phi_2(\mu)|^2\\
+\lambda^4\big(\Gamma_N^2+\mu^2\big)\big(\Gamma_S^2-\Gamma_N^2-\mu^2\big)\big]/|\phi_3|^2,
\end{aligned}\tag{47}$$

where $\phi_2(\mu)=\prod_{j=3,4,5}(i\mu-s_j)$, $\phi_1(\mu)=(i\mu+\Gamma_N)\phi_2(\mu)$, and $\phi_3(\mu)=\prod_{j=1,2,6,7,8}(i\mu-s_j)$. We can approximately evaluate $G_\uparrow$, taking into consideration only the first term appearing in Eq. (47). From this analysis, we can determine positions of peaks in the differential conductance. We observe two peaks at positive and two peaks at negative bias voltage. The internal peaks at $eV=\pm\Gamma_S$ hardly depend on λ, whereas the outer peaks appear at $eV\simeq\pm(\Gamma_S^2+2\lambda^2)^{1/2}$. Moreover, the spectral weight of the internal peaks varies from 1 (for $\lambda=0$) to 0.5 (for stronger couplings λ). At the same time, the spectral weight of the outer peaks at $eV=\pm(\Gamma_S^2+2\lambda^2)^{1/2}$ increases to 1 (for $\lambda\geqslant 1$).

The time-dependent differential conductance shown Fig. 8 and its asymptotic limit (Fig. 9) provide information about the Andreev-type states of QD_1 (due to superconducting proximity effect) obtained for the special case, when the energy level $\varepsilon_1=0$ coincides with the zero-energy Majorana mode. Under such circumstances, the influence of the Majorana mode on the quasiparticle spectrum of QD_1 is manifested

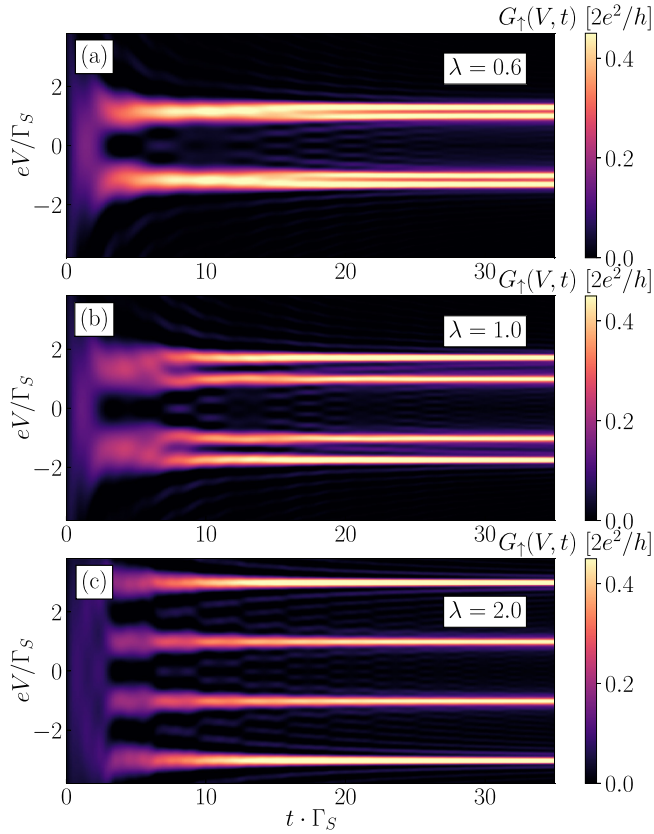

FIG. 8. The time-resolved differential conductance of the charge current flowing through the first quantum dot (QD_1) induced by the voltage bias V applied between the normal and superconducting leads. The consecutive panels refer to the different couplings $\lambda \equiv \lambda_1 = \lambda_2$, as indicated. The other parameters are the same as in Fig. 2 with $\Gamma_N = 0.2$.

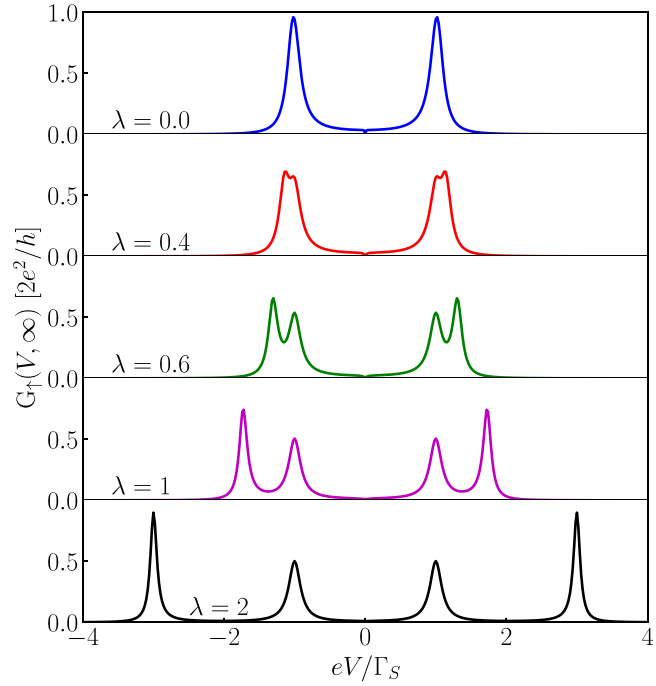

FIG. 9. The steady-state limit of the differential conductance $G_\uparrow(V,\infty)$ obtained for $\varepsilon_1 = \varepsilon_2 = 0$ and several values of $\lambda \equiv \lambda_1 = \lambda_2$, as indicated. The other parameters are the same as in Fig. 8.

by destructive quantum interference in analogy to Fano-type lineshapes appearing in double quantum dot T-shaped configurations [52–54]. Here, QD_1 is at the interface between the superconducting and normal leads with the side-attached Majorana mode, playing the role of "second quantum dot." Electrons moving between external leads can hop aside to the zero-energy level of the nanowire and return with a different phase, giving rise to destructive quantum interference, thereby depleting the spectral function of QD_1 near $\omega = \varepsilon_1$. Such a situation is no longer present for $\varepsilon_1 \neq 0$ because the side-attached Majorana mode has nothing to interfere with. In the present case, this destructive interference shows up as a tiny dip at zero voltage for a weakly coupled heterostructure (see the curves presented in Fig. 9 for $\lambda = 0.4$ and $\lambda = 0.6$).

In the remaining part of this section, we investigate the quasiparticle features appearing in the conductance $G_\uparrow(\mu,t)$ for $\varepsilon_1 \neq 0$, while $\varepsilon_2 = 0$. In such a situation the Majorana mode has a constructive influence on the transport properties, inducing the zero-energy quasiparticle which enhances the zero-bias conductance. This effect resembles a typical Majorana leakage on the quantum dot hybridized to the normal (metallic) electrodes [27–38]. For nonzero ε_1, we obtain

$$
\begin{aligned}
G_\uparrow(\mu,t) = 2\Gamma_N \mathrm{Re}\Bigg[& e^{-i\mu t}\mathcal{L}^{-1}\left\{\frac{(s+i\varepsilon+\Gamma_N)F_1(s)}{(s-i\mu)F_2(s)}\right\}(t)\Bigg] \\
& - 2\Gamma_N^2\Bigg[\left|\mathcal{L}^{-1}\left\{\frac{(s+i\varepsilon+\Gamma_N)F_1(s)}{(s-i\mu)F_2(s)}\right\}(t)\right|^2 \\
& + \Gamma_S^2\lambda_1^4\left|\mathcal{L}^{-1}\left\{\frac{s+i\varepsilon+\Gamma_N}{(s-i\mu)F_2(s)}\right\}(t)\right|^2 \\
& - \Gamma_S^2\left|\mathcal{L}^{-1}\left\{\frac{F_1(s)}{(s+i\mu)F_2(s)}\right\}(t)\right|^2 \\
& - \lambda_1^4\left|\mathcal{L}^{-1}\left\{\frac{(s+\Gamma_N)^2+\varepsilon^2}{(s+i\mu)F_2(s)}\right\}(t)\right|^2\Bigg],
\end{aligned}
\tag{48}
$$

where $F_1(s) = s^3 + 2\Gamma_N s^2 + s(\varepsilon^2 + \Gamma_S^2 + \Gamma_N^2 + \lambda_1^2) - \lambda_1^2(i\varepsilon - \Gamma_N)$ and $F_2(s) = (s^2 + 2\Gamma_N s + \varepsilon^2 + \Gamma_S^2 + \Gamma_N^2)[s^3 + 2\Gamma_N s^2 + s(\Gamma_N^2 + \varepsilon^2 + \Gamma_S^2 + 2\lambda_1^2) + 2\lambda_1^2\Gamma_N]$.

Figure 10 shows the time-dependent differential conductance $G_{1\uparrow}(V,t)$ obtained for nonzero value of the QD_1 energy level, $\varepsilon_1 = 2$, and several values of the coupling λ, as indicated. In the stationary limit ($t \to \infty$), the height of the zero-energy peak tends to 0.5, which is a typical fractional value initially predicted for the leaking Majorana mode [22,27,28] for arbitrary λ. Its width increases here upon increasing the coupling λ, as can be also seen in the stationary limit presented in Fig. 11, which displays the behavior of the differential conductance in the stationary limit.

To estimate the time interval in which the zero-energy Majorana mode leaks onto QD_1 we introduce a

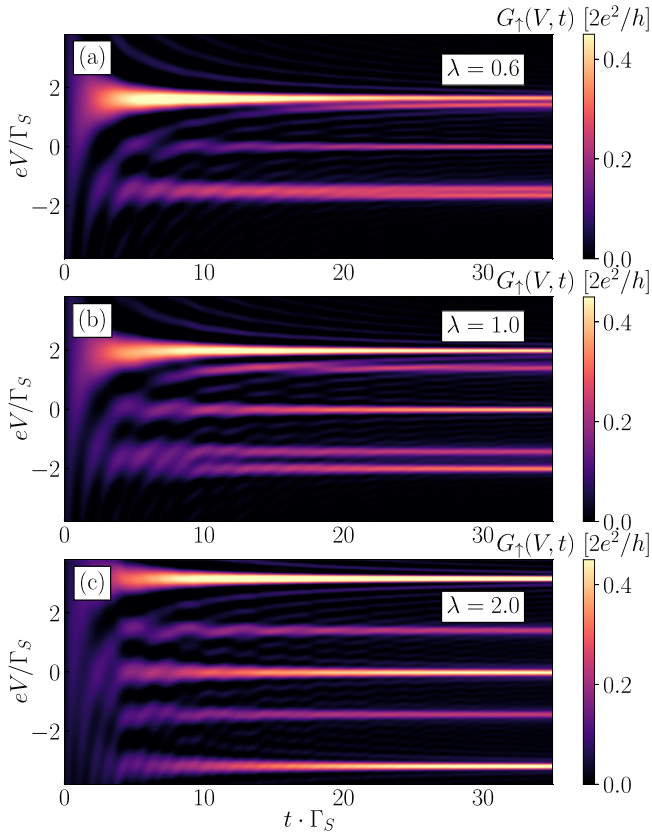

FIG. 10. The time-dependent differential conductance $G_\uparrow(V,t)$ obtained for nonzero energy level of the first quantum dot, $\varepsilon_1 = 2$, while $\varepsilon_2 = 0$, and for different values of the coupling λ, as indicated. The other parameters are the same as in Fig. 8.

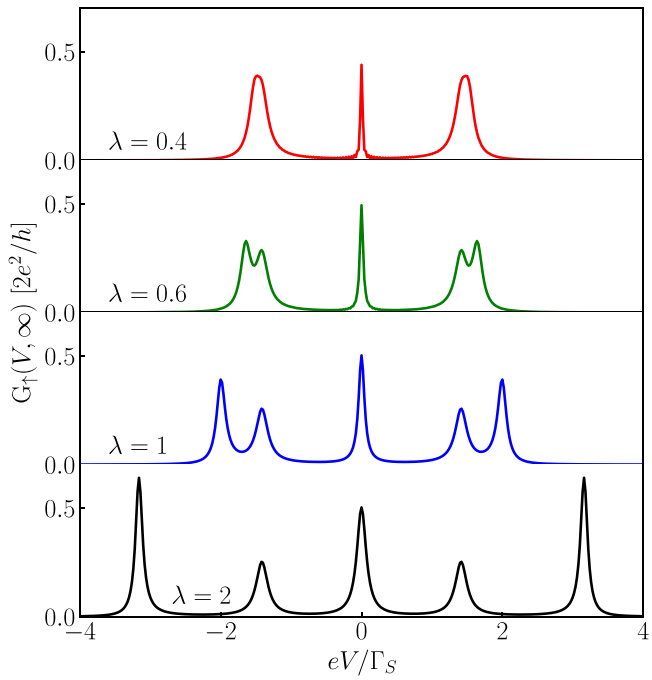

FIG. 11. The steady-state limit of the differential conductance $G_\uparrow(V, t = \infty)$ obtained for several values of λ (as indicated) and the other parameters the same as in Fig. 10.

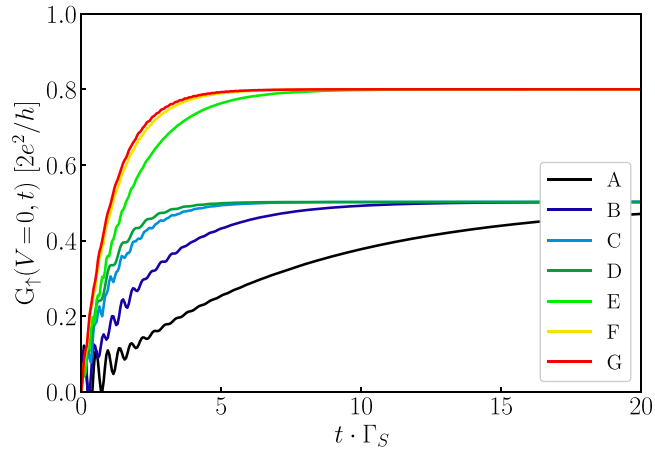

FIG. 12. The zero-bias differential conductance $G_\uparrow(V = 0, t)$ varying against time for $\varepsilon_1 = 1$ (A, B, C, D curves) and $\varepsilon_1 = 2$ (E, F, G lines) using different values of λ listed in Table I. The other parameters are the same as in Fig. 10.

phenomenological parameter τ defined by [43]

$$G_\uparrow(0,t) = G_\uparrow(0,\infty)[1 - e^{t/\tau}]. \tag{49}$$

This parameter characterizes the timescale, over which the zero-bias conductance approaches the stationary limit value $G_\uparrow(0,\infty)$. We computed τ for two different values of energy levels ε_1 (while $\varepsilon_2 = 0$) and several values of the coupling λ. Figure 12 presents the zero-bias conductance $G_\uparrow(V = 0, t)$ for $\varepsilon_1 = 1$ (A, B, C, D curves) and $\varepsilon_1 = 2$ (E, F, G lines), using λ specified in Table I. We found $\tau \approx 7.5, 2.5, 1.25, 1.0$ (expressed in units of $\frac{1}{\Gamma_N}$) for the couplings $\lambda = 0.4$, 0.8, 2, and 8, respectively. Similarly, for the other value of the energy level, $\varepsilon_1 = 2$, we estimated the leakage timescales $\tau \approx 1.6$, 1.15, 1.1. We thus conclude that the development of the zero-energy Majorana mode on QD_1 occurs faster upon increasing the coupling to topological superconductor λ.

Summarizing this section, we emphasize that quasiparticles emerging on QD_1 (presented in Figs. 10 and 11) represent the trivial Andreev bound states (at finite voltage V) coexisting with the topological (zero-bias) feature. Their formation occurs over some characteristic timescale τ [see Table I] and is accompanied by the damped quantum oscillations. Buildup of the quasiparticles is predominantly controlled by the coupling of QD_1 to a continuous spectrum of the metallic lead, but spectral weights and energies of such quasiparticles

TABLE I. The timescale τ of the Majorana leakage obtained for several couplings $\lambda \equiv \lambda_1 = \lambda_2$ and different values of the first quantum dot energy level ε_1 with $\varepsilon_2 = 0$.

Curve	$\lambda[\Gamma_S]$	$\varepsilon_1[\Gamma_S]$	$\tau[1/\Gamma_N]$
A	0.4	1	7.5
B	0.8	1	2.5
C	2.0	1	1.25
D	8.0	1	1.0
E	2.0	2	1.6
F	4.0	2	1.15
G	6.0	2	1.1

depend on the energy level ε_1 of QD_1, what indirectly affects the profile of damped quantum oscillations observed in the transient regime.

Let us also comment about the characteristic energy and timescales of our setup which could be verified empirically. Topological superconductivity of the semiconducting nanowires and magnetic nanochains has been so far achieved by contacting them with the conventional superconductors, such as Al or Pb whose pairing gaps (safely below T_c) are about 0.5 meV. The topological gap (which separates the zero-energy Majorana modes from the trivial bound states) is even smaller, on the order of 0.1–0.2 meV. This establishes the typical energy scale for our hybrid system, because within the effective low-energy description (4) we consider only the Majorana modes of nanowire, neglecting any other (higher-energy) trivial bound states. As far as the coupling Γ_S of QD_1 is concerned, we assume it to be at most comparable to the topological gap of the nanowire (because otherwise QD1 would hybridize with trivial states of the nanowire). The other coupling $\Gamma_N = 0.1\Gamma_S$, controlling the relaxation processes, is on the order of 10 μeV. Under such conditions the typical transient region would extend from a fraction to a few nanoseconds (for more detailed quantitative evaluations for the single dot topological superconductor hybrid structure, see Ref. [43]).

V. CORRELATION EFFECTS

Finally, we address the role played by the Coulomb repulsion $U\hat{n}_{i\uparrow}\hat{n}_{i\downarrow}$, which can be expected to suppress the superconducting proximity effect. We study its influence both on the local and nonlocal electron pairings. For a single quantum dot attached to superconductor, this issue has been extensively studied, considering the static [55,56] and nonequilibrium conditions [57–60]. Depending on the ratio of Γ_S/U and the energy level, the quantum dot was predicted to be either singly occupied or in the BCS-type configuration. The superconducting proximity effect is efficient only in the latter case. In this section we analyze effects of the Coulomb repulsion on the time-dependent pairings in the transient region and in asymptotic behavior of our hybrid structure (Fig. 1).

To accurately describe the correlation effects and system's dynamics, we resort to the numerical renormalization group (NRG) method [61–63]. This method has been successfully used to analyze the stationary properties of the Anderson impurity coupled to superconductor [55,64]. Here, we make use of its time-dependent extension [65–67] to address the dynamical effects of our setup. The main idea of the NRG approach is a logarithmic discretization of the conduction band, which allows one to map the Hamiltonian to a chain-like form. Matrix Hamiltonian of such a model can be next diagonalized in an iterative fashion, keeping an appropriate number of the low-energy states. This technique can be used to determine the time-dependent physical observables and is not limited by perturbative approximations (for details see, e.g., Refs. [65–67]).

In Fig. 13 we present the time-dependent local electron pairings $C_{11}(t) = \langle d_{1\downarrow}(t)d_{1\uparrow}(t)\rangle$ obtained for the half filled quantum dots $\varepsilon_i = -U/2$ and different values of Γ_S/U. In this figure the quench is performed in all the couplings, i.e.,

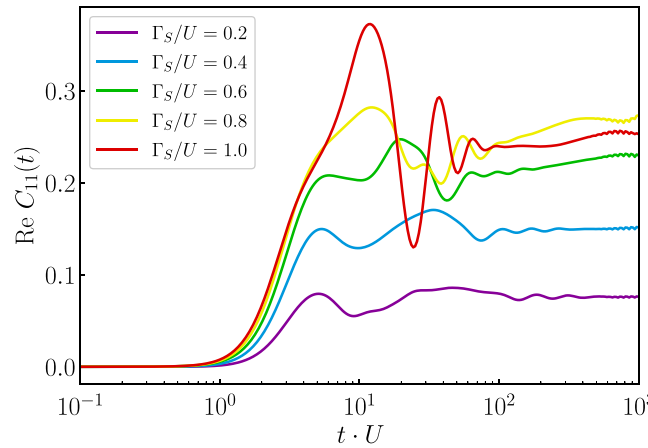

FIG. 13. The real part of $C_{11}(t) = \langle d_{1\downarrow}(t)d_{1\uparrow}(t)\rangle$ obtained by time-dependent NRG calculations for the half filled quantum dots $\varepsilon_1 = \varepsilon_2 = -U/2$, assuming $\Gamma_N/U = 0.1$ and $\lambda/U = 0.2$ ($\lambda \equiv \lambda_1 = \lambda_2$), with $U = 1$, and different values of Γ_S, as indicated. Energies are now expressed in terms of band half-width.

the couplings to both leads and topological superconductor. To identify temporal extent of the transient region, we plot all observables against the logarithm of time. First of all, one can notice that transient phenomena start developing when $t \gtrsim 1/U$ and are most important for timescales coinciding roughly with $t \sim 1/\Gamma_N$. Moreover, a closer inspection of the local electron pairing induced on QD_1 reveals its substantial suppression caused by the Coulomb repulsion. This tendency is consistent with the steady-state solution for N-QD_1-S nanostructure [55,64]. The reduction of the local electron pairing is associated with ensuing changeover of the quantum dot ground state, from the BCS-type to the singly occupied configuration. In the absence of the topological superconductor ($\lambda = 0$) such quantum phase transition would occur at $\Gamma_S/U = 0.5$ [55]. However, the influence of the side-attached topological superconductor partly smears this singlet-doublet phase transition in our setup [35,36].

Let us now focus on the dynamics of the triplet pairing $C_{2f}(t) = \langle \hat{d}_{2\uparrow}(t)\hat{f}(t)\rangle$, which is presented in Fig. 14. To analyze its behavior, we fix the couplings to the normal and superconducting contacts and perform quench only in the coupling to topological superconductor. The upper panel presents the evolution of the real part of $C_{2f}(t)$ for different values of the couplings to topological superconductor in the case of $\varepsilon_M = 0$, while the bottom panel shows the imaginary part of $C_{2f}(t)$ for one selected value of λ, while assuming finite ε_M, as indicated. We first notice that the mixed (triplet) pairing, in contrast with the local pairing induced at QD_1, hardly depends on Γ_S. This property indicates that the leakage of the Majorana mode on the side-attached quantum dots is not endangered by the interplay of correlations and superconducting pairing on the first quantum dot. Finite $C_{2f}(t)$ starts developing when $t \gtrsim 1/U$, showing considerable oscillations for $t \gtrsim 1/\Gamma_N$, which however die out at longer times. As can be seen, the amplitude of these oscillations increases with raising coupling to topological superconductor λ, giving rise to larger value of $C_{2f}(t)$ in the long time limit, see Fig. 14(c). On the other hand, the imaginary part of $C_{2f}(t)$ shows

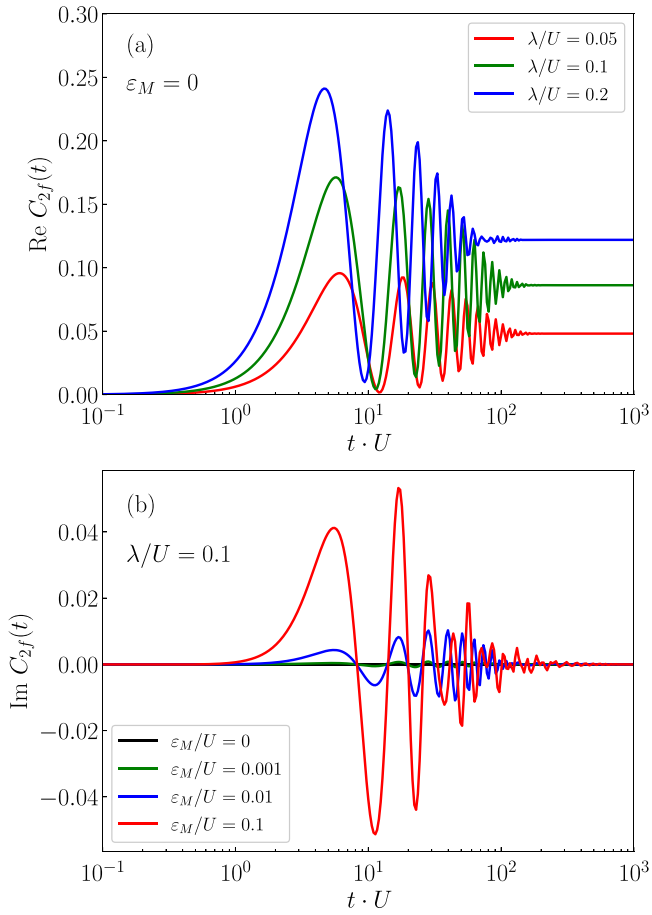

FIG. 14. The variation of the (a) real and (b) imaginary parts of $C_{2f}(t)$ obtained by time-dependent NRG calculations for the half-filled quantum dots $\varepsilon_1 = \varepsilon_2 = -U/2$, assuming $\Gamma_N/U = 0.1$, coupling $\Gamma_S/U = 0.75$ and different values of (a) $\lambda \equiv \lambda_1 = \lambda_2$ and (b) the overlap between the Majorana modes ε_M, as indicated.

considerable oscillations in the transient regime only when there is a finite overlap between Majorana modes (the real part hardly depends on ε_M), see Fig. 14(b). The amplitude of these oscillations increases with ε_M, indicating a nonlocal character of Majorana quasiparticles in the transient regime.

VI. SUMMARY AND OUTLOOK

We have studied the local and nonlocal transient phenomena of a hybrid structure composed of two quantum dots attached on opposite sides to the topological superconducting nanowire. We have shown that in a steady-state limit these spatially distant quantum dots interconnected through the Majorana edge-modes develop the quasiparticle spectra independent of one another. Despite the lack of static cross-correlations, however, we have found dynamical nonlocal effects transmitted between the dots surviving over a finite time interval. These effects are apparent in the interdot electron pairing, both for the singlet and triplet channels, which could be detectable in the crossed Andreev reflection spectroscopy.

We have also investigated gradual development of the quasiparticle states of QD_1 (placed) on interface between the normal and conventional superconductor), focusing on signatures of the Majorana mode. We have found coexistence of the Andreev (trivial) bound states with the zero-energy (topological) feature. Emergence of these quasiparticles can be empirically verified by time-resolved differential conductance of the tunneling current induced across QD_1 by the bias voltage between the external metallic and superconducting leads. For the zero energy level $\varepsilon_1 = 0$, the Majorana mode imprints a tiny dip at zero voltage, originating from its destructive quantum interference on the spectrum of QD_1. This effect is analogous to the Fano-type interference observed in T-shaped configurations of double quantum dot junctions [52–54]. Otherwise, i.e. for $\varepsilon_1 \neq 0$, the Majorana mode induces the zero-energy conductance peak. In the latter case the leakage of the Majorana mode yields a fractional value of the zero-bias differential conductance, Fig. 11. We have also studied the effect of Coulomb interactions on the transient phenomena and revealed their destructive influence on the local (on-dot) pairing.

Our analysis relied on the assumption of very large pairing gap Δ_{SC} of the superconducting lead. In realistic situations one should additionally take into account the electronic states from outside this pairing gap, which for conventional superconductors is typically a fraction of meV. The influence of such continuum has been discussed for superconducting nanostructures, using various many-body techniques [57,58,60,68–71] suitable to capture also the correlation effects. These methods could be adopted to the present setup as well. In general, the quasiparticles from outside the pairing gap would contribute to the relaxation processes, partly reducing the relevant timescales characterizing the transient phenomena. Another important issue could be associated with qualitative changeover of the trivial (Andreev) and topological (Majorana) states imposed by the quantum quenches [39,41]. Postquench evolution could lead to the dynamical phase transition [59], but this challenging topic is beyond the scope of the present study.

For possible verification, we have evaluated the timescale needed for emergence of the trivial (Andreev) and topological (Majorana) bound states. In typical realizations of superconducting hybrid structures (where the couplings $\Gamma_{N,S}$ of the quantum dots to external leads are $\approx$ meV) the duration of the transient effects would cover nanoseconds region. Currently available tunneling spectroscopies [72] should be able to detect the nonlocal cross-correlations between the spatially distant quantum dots embedded into the setup presented in Fig. 1. Detection of transient nonlocal pairing in the singlet $C_{12}(t)$ and triplet $C_{12}^{\mathrm{T}}(t)$ channel could be obtained by crossed Andreev spectroscopy, analogous to the methods used recently in the minimal-length topological superconducting system [11,12]. As concerns the triplet channel, its measurement would be feasible by means of the equal spin electron-to-hole scattering [73]. Time-resolved nonlocal spectroscopy could be done for the hybrid structure, using either semiconducting nanowires (e.g., InAs) partly covered by conventional superconductors (like in the setup reported in Ref. [26]) or by depositing magnetic atoms (Fe) on superconductors and attaching other nonmagnetic impurities to them that can be probed by scanning spin-polarized Andreev spectroscopy [74]. Detailed knowledge of such transient nonlocal

effects might be useful for reliable control of braiding protocols for conventional and/or topological superconducting quantum bits [75,76].

Finally, we would like to mention that it would be worthwhile to extend the present analysis of the nonlocal transient phenomena onto hybrid structures with quasi-Majorana states. These quasiparticles have been predicted to form at the boundaries of semiconducting nanowires proximitized to superconducting materials, due to a flat confining potential [77], a suppressed superconducting pair potential and/or an excess Zeeman field [78] or attachment of quantum dot(s) [79]. Under such circumstances the trivial Andreev states appear at nearly zero energy, and their properties, such as, e.g., the zero-bias conductance peak [80,81], the fractional Josephson effect [82], and the braiding schemes [83], very much resemble the behavior of true Majorana modes. In static situations, it is rather difficult to discern whether the zero-energy edge modes have their trivial or topological origin [84,85]. However, the theoretical results reported in Ref. [40] seem to indicate that the true Majorana modes could be unambiguously manifested by the characteristic quantum oscillations in time-dependent conductance right after applying a source-drain voltage, which otherwise would not occur for the trivial modes. In this regard, a follow-up in-depth study of the nonlocal transient effects for quasi-Majorana modes in similar hybrid devices as considered here would be desirable.

ACKNOWLEDGMENTS

This work was supported by the National Science Centre in Poland through the Project No. 2018/29/B/ST3/00937. K.W. acknowledges financial support by the National Science Centre in Poland through the Project No. 2022/45/B/ST3/02826. We acknowledge the computing time at the Poznań Supercomputing and Networking Center. We thank T. Kwapiński and B. Baran for technical assistance.

APPENDIX A: TIME-DEPENDENT EXPECTATION VALUES

To calculate the electron occupancy of QD_1 embedded in the uncorrelated setup we use the expression (8) for $\hat{d}_{1\uparrow}(s)$ and obtain

$$\begin{aligned}
n_{1\uparrow}(t) &= \langle \mathcal{L}^{-1}\{\hat{d}^\dagger_{1\uparrow}(s)\}\mathcal{L}^{-1}\{\hat{d}_{1\uparrow}(s)\}\rangle \\
&= [1-n_{1\uparrow}(0)]\lambda_1^4\left(\mathcal{L}^{-1}\left\{\frac{(s+\Gamma_N)^2}{H_3(s)}\right\}(t)\right)^2 + n_{1\uparrow}(0)\left(\mathcal{L}^{-1}\left\{\frac{(s+\Gamma_N)H_1(s)}{H_3(s)}\right\}(t)\right)^2 + [1-n_{1\downarrow}(0)]\Gamma_S^2\left(\mathcal{L}^{-1}\left\{\frac{H_1(s)}{H_3(s)}\right\}(t)\right)^2 \\
&\quad + n_{1\downarrow}(0)\Gamma_S^2\lambda_1^4\left(\mathcal{L}^{-1}\left\{\frac{s+\Gamma_N}{H_3(s)}\right\}(t)\right)^2 + \langle \hat{f}^\dagger(0)+\hat{f}(0)\rangle\langle \hat{f}(0)+\hat{f}^\dagger(0)\rangle\frac{\lambda_1^2}{2}\left(\mathcal{L}^{-1}\left\{\frac{(s+\Gamma_N)}{H_2(s)}\right\}(t)\right)^2 \\
&\quad + \sum_{\mathbf{k},\mathbf{k}_1} V_{\mathbf{k}}V_{\mathbf{k}_1}\langle \mathcal{L}^{-1}\{S^\dagger_{\mathbf{k}}(s)\}(t)\mathcal{L}^{-1}\{S_{\mathbf{k}_1}(s)\}(t)\rangle, \qquad \text{(A1)}
\end{aligned}$$

where $H_1(s)$, $H_2(s)$, $H_3(s)$, and $S_{\mathbf{k}}(s)$ are defined in Eqs. (10), (11), (12), and (15). The first five terms can be rewritten in the form given by Eq. (17) and calculation of the last term can be performed as follows:

$$\begin{aligned}
&\sum_{\mathbf{k},\mathbf{k}_1} V_{\mathbf{k}}V_{\mathbf{k}_1}\left\langle \mathcal{L}^{-1}\left\{\Gamma_S\frac{\hat{c}_{\mathbf{k}\downarrow}(0)H_1(s)}{(s+i\varepsilon_{\mathbf{k}})H_3(s)} + i\frac{\hat{c}^\dagger_{\mathbf{k}\uparrow}(0)(s+\Gamma_N)H_1(s)}{(s-i\varepsilon_{\mathbf{k}})H_3(s)} + \Gamma_S\lambda_1^2\frac{\hat{c}^\dagger_{\mathbf{k}\downarrow}(0)(s+\Gamma_N)}{(s-i\varepsilon_{\mathbf{k}})H_3(s)} - i\lambda_1^2\frac{\hat{c}_{\mathbf{k}\uparrow}(0)(s+\Gamma_N)^2}{(s+i\varepsilon_{\mathbf{k}})H_3(s)}\right\}(t)\right. \\
&\quad \left.\times\,\mathcal{L}^{-1}\left\{\Gamma_S\frac{\hat{c}^\dagger_{\mathbf{k}_1\downarrow}(0)H_1(s)}{(s-i\varepsilon_{\mathbf{k}_1})H_3(s)} - i\frac{\hat{c}_{\mathbf{k}_1\uparrow}(0)(s+\Gamma_N)H_1(s)}{(s+i\varepsilon_{\mathbf{k}_1})H_3(s)} + \Gamma_S\lambda_1^2\frac{\hat{c}_{\mathbf{k}_1\downarrow}(0)(s+\Gamma_N)}{(s+i\varepsilon_{\mathbf{k}_1})H_3(s)} + i\lambda_1^2\frac{\hat{c}^\dagger_{\mathbf{k}_1\uparrow}(0)(s+\Gamma_N)^2}{(s-i\varepsilon_{\mathbf{k}_1})H_3(s)}\right\}(t)\right\rangle \\
&= \sum_{\mathbf{k},\mathbf{k}_1} V_{\mathbf{k}}V_{\mathbf{k}_1}\left\{\Gamma_S^2\langle\hat{c}_{\mathbf{k}\downarrow}(0)\hat{c}^\dagger_{\mathbf{k}_1\downarrow}(0)\rangle\mathcal{L}^{-1}\left\{\frac{H_1(s)}{(s+i\varepsilon_{\mathbf{k}})H_3(s)}\right\}(t)\mathcal{L}^{-1}\left\{\frac{H_1(s)}{(s-i\varepsilon_{\mathbf{k}_1})H_3(s)}\right\}(t) + \langle\hat{c}^\dagger_{\mathbf{k}\uparrow}(0)\hat{c}_{\mathbf{k}_1\uparrow}(0)\rangle\mathcal{L}^{-1}\left\{\frac{(s+\Gamma_N)H_1(s)}{(s-i\varepsilon_{\mathbf{k}})H_3(s)}\right\}(t)\right. \\
&\quad \times\,\mathcal{L}^{-1}\left\{\frac{(s+\Gamma_N)H_1(s)}{(s+i\varepsilon_{\mathbf{k}_1})H_3(s)}\right\}(t) + \Gamma_S^2\lambda_1^4\langle\hat{c}^\dagger_{\mathbf{k}\downarrow}(0)\hat{c}_{\mathbf{k}_1\downarrow}(0)\rangle\mathcal{L}^{-1}\left\{\frac{(s+\Gamma_N)}{(s-i\varepsilon_{\mathbf{k}})H_3(s)}\right\}(t)\mathcal{L}^{-1}\left\{\frac{(s+\Gamma_N)}{(s+i\varepsilon_{\mathbf{k}_1})H_3(s)}\right\}(t) \\
&\quad \left.+\,\lambda_1^4\langle\hat{c}_{\mathbf{k}\uparrow}(0)\hat{c}^\dagger_{\mathbf{k}_1\uparrow}(0)\rangle\mathcal{L}^{-1}\left\{\frac{(s+\Gamma_N)^2}{(s+i\varepsilon_{\mathbf{k}})H_3(s)}\right\}(t)\mathcal{L}^{-1}\left\{\frac{(s+\Gamma_N)^2}{(s-i\varepsilon_{\mathbf{k}_1})H_3(s)}\right\}(t)\right\} \\
&= \frac{\Gamma_N}{\pi}\int_{-\infty}^{\infty}d\varepsilon\left\{\Gamma_S^2[1-f_N(\varepsilon)]\mathcal{L}^{-1}\left\{\frac{H_1(s)}{(s+i\varepsilon)H_3(s)}\right\}(t)\mathcal{L}^{-1}\left\{\frac{H_1(s)}{(s-i\varepsilon)H_3(s)}\right\}(t) + f_N(\varepsilon)\mathcal{L}^{-1}\left\{\frac{(s+\Gamma_N)H_1(s)}{(s-i\varepsilon)H_3(s)}\right\}(t)\right. \\
&\quad \times\,\mathcal{L}^{-1}\left\{\frac{(s+\Gamma_N)H_1(s)}{(s+i\varepsilon)H_3(s)}\right\}(t) + \Gamma_S^2\lambda_1^4 f_N(\varepsilon)\mathcal{L}^{-1}\left\{\frac{(s+\Gamma_N)}{(s-i\varepsilon)H_3(s)}\right\}(t)\mathcal{L}^{-1}\left\{\frac{(s+\Gamma_N)}{(s+i\varepsilon)H_3(s)}\right\}(t) \\
&\quad \left.+\,\lambda_1^4[1-f_N(\varepsilon)]\mathcal{L}^{-1}\left\{\frac{(s+\Gamma_N)^2}{(s+i\varepsilon)H_3(s)}\right\}(t)\mathcal{L}^{-1}\left\{\frac{(s+\Gamma_N)^2}{(s-i\varepsilon)H_3(s)}\right\}(t)\right\}. \qquad \text{(A2)}
\end{aligned}$$

This expression can be simply transformed to the form given in Eq. (17).

Performing similar calculations for $n_{1\downarrow}(t)$ we obtain

$$n_{1\downarrow}(t) = n_{1\uparrow}(0)N_{\uparrow}(t) + n_{1\downarrow}(0)N_{\downarrow}(t) + N(t) + \frac{\Gamma_N}{\pi}\int_{-\infty}^{\infty} d\varepsilon[f_N(\varepsilon)\Psi_1(\varepsilon,t) + \Psi_2(\varepsilon,t)], \tag{A3}$$

where

$$N_{\uparrow}(t) = \Gamma_S^2\lambda_1^4\left(\mathcal{L}^{-1}\left\{\frac{(s+\Gamma_N)^2}{H_3(s)}\right\}(t)\right)^2 - \Gamma_S^2\left(\mathcal{L}^{-1}\left\{\frac{H_1(s)}{H_3(s)}\right\}(t)\right)^2, \tag{A4}$$

$$N_{\downarrow}(t) = \left(\mathcal{L}^{-1}\left\{\frac{\Gamma_S^2 H_1(s)}{(s+\Gamma_N)H_3(s)} - \frac{1}{s+\Gamma_N}\right\}(t)\right)^2 - \Gamma_S^2\lambda_1^4\left(\mathcal{L}^{-1}\left\{\frac{1}{H_3(s)}\right\}(t)\right)^2, \tag{A5}$$

$$N(t) = \Gamma_S^2\left(\mathcal{L}^{-1}\left\{\frac{H_1(s)}{H_3(s)}\right\}(t)\right)^2 + \Gamma_S^4\lambda_1^4\left(\mathcal{L}^{-1}\left\{\frac{1}{H_3(s)}\right\}(t)\right)^2 + \frac{\Gamma_S^2\lambda_1^2}{2}\left(\mathcal{L}^{-1}\left\{\frac{1}{H_2(s)}\right\}(t)\right)^2, \tag{A6}$$

and

$$\begin{aligned}\Psi_1(\varepsilon,t) = {}& \Gamma_S^2\lambda_1^4\left|\mathcal{L}^{-1}\left\{\frac{s+\Gamma_N}{(s+i\varepsilon)H_3(s)}\right\}(t)\right|^2 - \Gamma_S^2\lambda_1^4\left|\mathcal{L}^{-1}\left\{\frac{1}{(s+i\varepsilon)H_3(s)}\right\}(t)\right|^2 \\ & + \left|\mathcal{L}^{-1}\left\{\left(\frac{\Gamma_S^2 H_1(s)}{(s+\Gamma_N)H_3(s)} - \frac{1}{s+\Gamma_N}\right)\frac{1}{s-i\varepsilon}\right\}(t)\right|^2 - \Gamma_S^2\left|\mathcal{L}^{-1}\left\{\frac{H_1(s)}{(s-i\varepsilon)H_3(s)}\right\}(t)\right|^2\end{aligned} \tag{A7}$$

$$\Psi_2(\varepsilon,t) = \Gamma_S^4\lambda_1^4\left|\mathcal{L}^{-1}\left\{\frac{1}{(s+i\varepsilon)H_3(s)}\right\}(t)\right|^2 + \Gamma_S^2\left|\mathcal{L}^{-1}\left\{\frac{H_1(s)}{(s+i\varepsilon)H_3(s)}\right\}(t)\right|^2. \tag{A8}$$

Note, that $n_{1\downarrow}(t)$ does not depend on λ_2 and ε_2.

The intradot pairing function (32) can be computed, using the Laplace transforms $\hat{d}_{1\uparrow}(s)$ and $\hat{d}_{1\downarrow}(s)$ expressed in equations (8) and (16). Following the procedure discussed above for the charge occupancies we finally obtain (assuming the initial empty dots)

$$\langle\hat{d}_{1\downarrow}(t)\hat{d}_{1\uparrow}(t)\rangle = D(t) + i\frac{\Gamma_N\Gamma_S}{\pi}\int_{-\infty}^{\infty}[f_N(\varepsilon)D_1(\varepsilon,t) + D_2(\varepsilon,t)], \tag{A9}$$

where

$$\begin{aligned}D(t) = i\Gamma_S\Bigg[{}& \lambda_1^4\mathcal{L}^{-1}\left\{\frac{s+\Gamma_N}{H_3(s)}\right\}(t)\mathcal{L}^{-1}\left\{\frac{(s+\Gamma_N)^2}{H_3(s)}\right\}(t) + \mathcal{L}^{-1}\left\{\frac{H_1(s)}{H_3(s)}\right\}(t)\mathcal{L}^{-1}\left\{\frac{\Gamma_S^2 H_1(s) - H_3(s)}{(s+\Gamma_N)H_3(s)}\right\}(t) \\ & + \frac{\lambda_1^2}{2}\mathcal{L}^{-1}\left\{\frac{1}{H_2(s)}\right\}(t)\mathcal{L}^{-1}\left\{\frac{s+\Gamma_N}{H_2(s)}\right\}(t)\Bigg],\end{aligned} \tag{A10}$$

$$\begin{aligned}D_1(\varepsilon,t) = {}& \lambda_1^4\mathcal{L}^{-1}\left\{\frac{s+\Gamma_N}{(s+i\varepsilon)H_3(s)}\right\}(t)\mathcal{L}^{-1}\left\{\frac{\Gamma_S^2 - (s+\Gamma_N)^2}{(s-i\varepsilon)H_3(s)}\right\}(t) \\ & + \mathcal{L}^{-1}\left\{\frac{H_1(s)}{(s-i\varepsilon)H_3(s)}\right\}(t)\mathcal{L}^{-1}\left\{\frac{(s+\Gamma_N)^2 H_1(s) - \Gamma_S^2 H_1(s) + H_3(s)}{(s+\Gamma_N)(s+i\varepsilon)H_3(s)}\right\}(t),\end{aligned} \tag{A11}$$

$$D_2(\varepsilon,t) = \lambda_1^4\mathcal{L}^{-1}\left\{\frac{s+\Gamma_N}{(s+i\varepsilon)H_3(s)}\right\}(t)\mathcal{L}^{-1}\left\{\frac{(s+\Gamma_N)^2}{(s-i\varepsilon)H_3(s)}\right\}(t) + \mathcal{L}^{-1}\left\{\frac{H_1(s)}{(s-i\varepsilon)H_3(s)}\right\}(t)\mathcal{L}^{-1}\left\{\frac{\Gamma_S^2 H_1(s) - H_3(s)}{(s+\Gamma_N)(s+i\varepsilon)H_3(s)}\right\}(t). \tag{A12}$$

APPENDIX B: TRANSITION PROBABILITIES FOR $\Gamma_N = 0$ CASE

In Sec. III B we have shown that the electron occupancy of QD_1 does not depend on the topological nanowire coupling to the second quantum dot. With this conclusion in mind, let us first consider a simplified version of our setup, $\lambda_2 = 0$, in order to determine the charge occupancy of the proximitized QD_1 side-attached to the Majorana nanowire (i.e., completely ignoring any influence of QD_2). We choose the basis states $|n_{1\uparrow}, n_{1\downarrow}, n_f\rangle$, where $n_{1\sigma}$ represents either the empty or occupied σ spin of QD_1 and n_f stands for the number of nonlocal fermion constructed from the Majorana quasiparticles.

For specific considerations, we assume the initial ($t \leqslant 0$) configuration to be empty $|0,0,0\rangle$. In what follows, we compute the time-dependent fillings after connecting the proximitized QD_1 to the topological nanowire. Expressing the time-dependent state vector by

$$\begin{aligned}|n_{1\uparrow}(t), n_{1\downarrow}(t), n_f(t)\rangle = {}& a_1(t)|0,0,0\rangle + a_2(t)|1,1,0\rangle \\ & + a_3(t)|0,1,1\rangle + a_4(t)|1,0,1\rangle,\end{aligned}$$

we solve the Schrödinger equation to find the probability coefficients $a_j(t)$ for $t > 0$. From straightforward calculations we obtain the following coefficients:

$$a_1(t) = \frac{1}{2}\left[\left(\frac{\Gamma_S}{\sqrt{\Gamma_S^2+2\lambda^2}}+1\right)\cos(t\sqrt{b}) - \left(\frac{\Gamma_S}{\sqrt{\Gamma_S^2+2\lambda^2}}-1\right)\cos(t\sqrt{c})\right], \quad \text{(B1)}$$

$$a_2(t) = \frac{i}{\sqrt{\Gamma_S^2+2\lambda^2}}[\sqrt{c}\sin(t\sqrt{c}) - \sqrt{b}\sin(t\sqrt{b})], \quad \text{(B2)}$$

$$a_3(t) = \frac{\lambda}{\sqrt{2\Gamma_S^2+(2\lambda)^2}}[\cos(t\sqrt{c}) - \cos(t\sqrt{b})], \quad \text{(B3)}$$

$$a_4(t) = \frac{i\lambda\sqrt{2}}{4}\left[\left(\frac{\Gamma_S}{\sqrt{\Gamma_S^2+2\lambda^2}}-1\right)\frac{\sin(t\sqrt{c})}{\sqrt{c}} - \left(\frac{\Gamma_S}{\sqrt{\Gamma_S^2+2\lambda^2}}+1\right)\frac{\sin(t\sqrt{b})}{\sqrt{b}}\right], \quad \text{(B4)}$$

where

$$b = \tfrac{1}{2}\left(\lambda^2+\Gamma_S^2+\Gamma_S\sqrt{\Gamma_S^2+2\lambda^2}\right)$$

and $$c = \tfrac{1}{2}\left(\lambda^2+\Gamma_S^2-\Gamma_S\sqrt{\Gamma_S^2+2\lambda^2}\right).$$

The time-dependent occupancies can be expressed in terms of these coefficients as

$$n_{1\uparrow}(t) = |a_2(t)|^2 + |a_4(t)|^2, \quad \text{(B5)}$$

$$n_{1\downarrow}(t) = |a_2(t)|^2 + |a_3(t)|^2, \quad \text{(B6)}$$

$$n_f(t) = |a_3(t)|^2 + |a_4(t)|^2, \quad \text{(B7)}$$

and they are consistent with Eqs. (25) and (26) obtained in the main part for the $\Gamma_N = 0$ case.

We can say that the formulas (B5)–(B7) resemble the Rabi oscillations of a four-level quantum system. In comparison with a two-level quantum system (realized when the uncorrelated quantum dot is coupled to superconducting lead in the limit of infinite pairing gap [49]) we observe here the oscillation of the state vector between four quantum states. We can describe the system evolution as an alternate oscillations between $|0,0,0\rangle$ and $|1,0,1\rangle$ (two upper curves in Fig. 15) and between $|0,1,1\rangle$ and $|1,1,0\rangle$ states (two lower curves in Fig. 15), respectively.

Note, that for the complete setup with both quantum dots the situation is more complicated because transitions would occur in larger basis $|n_{1\uparrow}, n_{1\downarrow}, n_f, n_{2\uparrow}\rangle$ comprising 16 possible configurations. Eight states correspond to even-parity and the other eight to odd-parity sectors. Assuming the initially empty state $|0,0,0,0\rangle$ we can express the latter state vector by a linear combination of the eight even-parity states with the corresponding time-dependent coefficients.

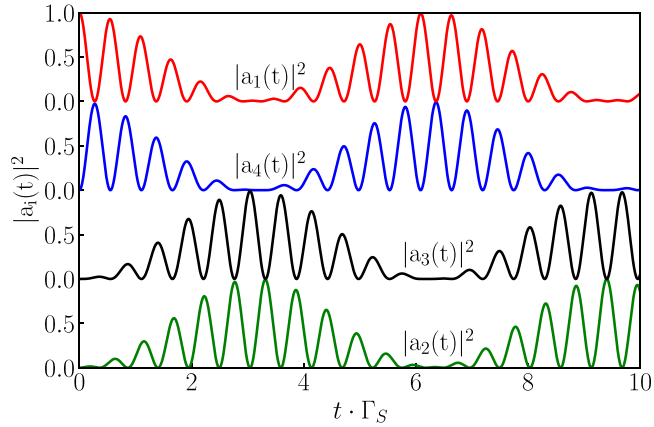

FIG. 15. Time-dependent probabilities $|a_j(t)|^2$ of a transition from the initial empty configuration to the state $|j\rangle$ defined in the basis $|n_{1\uparrow}, n_{1\downarrow}, n_f\rangle$ obtained for the limit of $\Gamma_N = 0$, $\lambda_1 = 8$, $\lambda_2 = 0$.

Introducing the auxiliary notation $|1\rangle = |0,0,0,0\rangle$, $|2\rangle = |1,0,0,0\rangle$, $|3\rangle = |0,1,0,0\rangle$, $|4\rangle = |1,1,0,0\rangle$, $|5\rangle = |0,0,1,0\rangle$, $|6\rangle = |1,0,1,0\rangle$, $|7\rangle = |0,1,1,0\rangle$, $|8\rangle = |1,1,1,0\rangle$, $|9\rangle = |0,0,0,1\rangle$, $|10\rangle = |1,0,0,1\rangle$, $|11\rangle = |0,1,0,1\rangle$, $|12\rangle = |1,1,0,1\rangle$, $|13\rangle = |0,0,1,1\rangle$, $|14\rangle = |1,0,1,1\rangle$, $|15\rangle = |0,1,1,1\rangle$, $|16\rangle = |1,1,1,1\rangle$, we

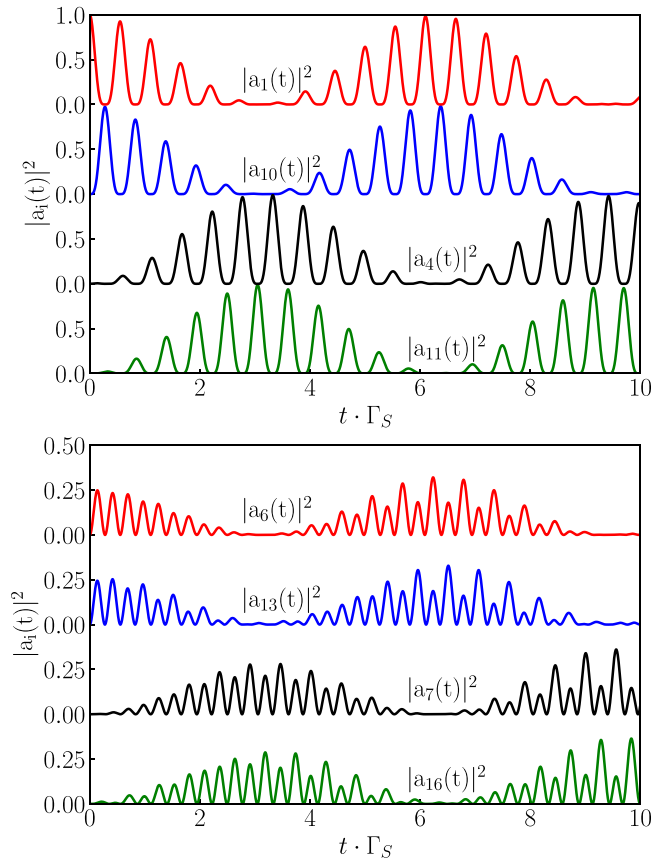

FIG. 16. Time-dependent probabilities $|a_j(t)|^2$ of a transition from the initial empty configuration to the state $|j\rangle$ defined in the basis $|n_{1\uparrow}, n_{1\downarrow}, n_f, n_{2\uparrow}\rangle$ obtained for $\Gamma_N = 0$, $\lambda_1 = \lambda_2 = 8$.

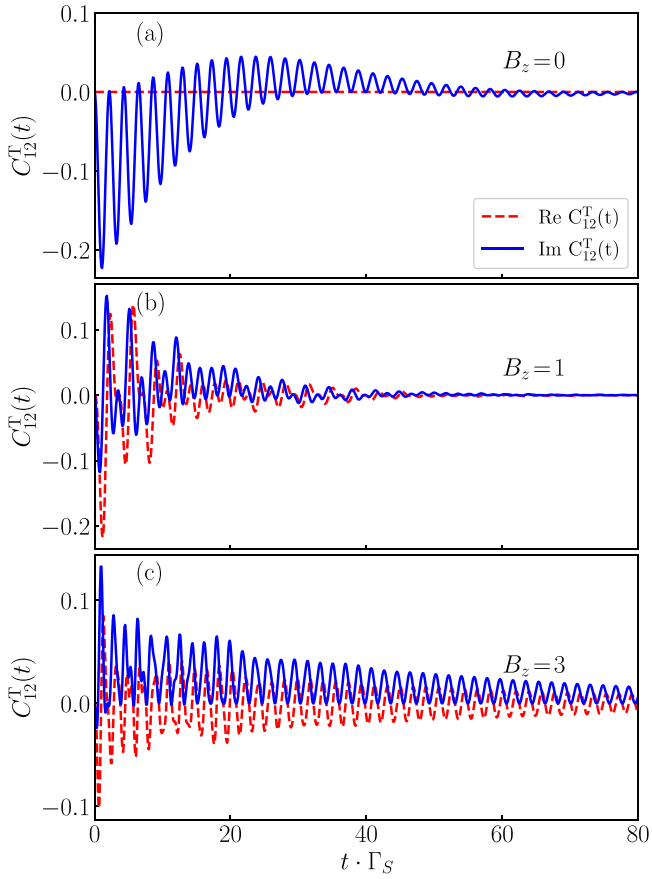

FIG. 17. Transient dynamics of the nonlocal pairing $C_{12}^{T}(t)$ in the triplet channel obtained for several values of the Zeeman field B_z, using the same set of model parameters as in Fig. 5.

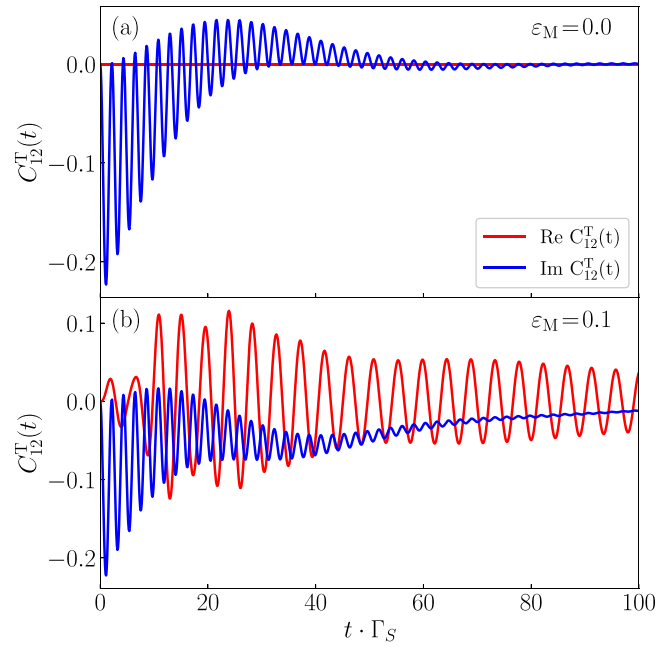

FIG. 18. Transient dynamics of the nonlocal pairing $C_{12}^{T}(t)$ in the triplet channel obtained for the nonoverlapping (upper panel) and overlapping Majorana modes (bottom panel), using the same model parameters as in Fig. 5.

can express the time-dependent occupancies of QD_1 as

$$n_{1\uparrow}(t) = |a_4(t)|^2 + |a_6(t)|^2 + |a_{10}(t)|^2 + |a_{16}(t)|^2, \quad \text{(B8)}$$

$$n_{1\downarrow}(t) = |a_4(t)|^2 + |a_7(t)|^2 + |a_{11}(t)|^2 + |a_{16}(t)|^2. \quad \text{(B9)}$$

The spin-↑ (spin-↓) occupancy of QD_1 indicates that at a given instant of time the system can be found in configurations with the occupied second quantum dot $|1, 0, 0, 1\rangle$ and $|1, 1, 1, 1\rangle$ ($|0, 1, 0, 1\rangle$ and $|1, 1, 1, 1\rangle$).

In Fig. 16 we plot the probabilities $|a_j(t)|^2$ for the corresponding states $|j\rangle$ as indicated. During the time evolution we observe clear oscillations between $|0, 0, 0, 0\rangle$ and $|1, 0, 0, 1\rangle$ states (two upper curves in upper panel in Fig. 16) and simultaneously oscillations between the states $|1, 1, 0, 0\rangle$ and $|0, 1, 0, 1\rangle$ (two lower curves in upper panel in Fig. 16).

From such considerations, we can also determine the pairing functions, expressing them by the complex coefficients $a_j(t)$. For the initial empty configuration, the on-dot pairing (32) takes the following form:

$$C_{11}(t) = a_1^{\star}(t)a_4(t) + a_{13}^{\star}(t)a_{16}(t), \quad \text{(B10)}$$

whereas for the initial odd-parity one obtains

$$C_{11}(t) = a_9^{\star}(t)a_{12}(t) + a_5^{\star}(t)a_8(t). \quad \text{(B11)}$$

In other words, the on-dot pairing function depends on the amplitude probabilities that the system evolving over all basis states can be found in states $|0, 0, 0, 0\rangle$, $|1, 1, 0, 0\rangle$, $|0, 0, 1, 1\rangle$, and $|1, 1, 1, 1\rangle$, respectively.

Similarly, we can determine the nonlocal pairing functions. For the initial empty configurations they are given by

$$C_{12}(t) = a_6^{\star}(t)a_{16}(t) - a_1^{\star}(t)a_{11}(t), \quad \text{(B12)}$$

$$C_{2f}(t) = a_4^{\star}(t)a_{16}(t) + a_1^{\star}(t)a_{13}(t). \quad \text{(B13)}$$

Note, that (B10) and (B13) depend on the same coefficients $a_j(t)$, but in different combinations.

APPENDIX C: NONLOCAL TRIPLET PAIRING

The leakage of Majorana modes onto the side-attached quantum dots is strictly related to the intersite triplet pairing between the outer sites of the topological nanowire and quantum dots. Within the present low-energy approach, such mechanism is captured by the mixed pairing $\langle \hat{d}_{i\uparrow}(t)\hat{f}(t)\rangle$, as discussed in Sec. III E. In this context, it is natural to explore the possible emergence of the nonlocal triplet pairing

$$C_{12}^{T}(t) = \langle \hat{d}_{1\uparrow}(t)\hat{d}_{2\uparrow}(t)\rangle \quad \text{(C1)}$$

because its efficiency might be detectable using the spin-polarized crossed Andreev reflection spectroscopy. Adopting our methodology to the nonlocal triplet pairing (C1), we obtain for $\varepsilon_{i\sigma} = 0$ and $\varepsilon_M = 0$

$$C_{12}^{T}(t) = \lambda_1\lambda_2\left(n_f(0) - \frac{1}{2}\right)\mathcal{L}^{-1}\left\{\frac{s+g}{H_2 s}\right\}(t) \times \mathcal{L}^{-1}\left\{\frac{1}{s^2 + 2\lambda_2^2}\right\}(t). \quad \text{(C2)}$$

In particular, for $\Gamma_N = 0$, this formula simplifies to

$$C_{12}^{\mathrm{T}}(t) = \frac{\lambda_1}{\sqrt{2\Delta^2 + 4\lambda_1^2}}\left(n_f(0) - \frac{1}{2}\right)\sin\left(\sqrt{2}\lambda_2 t\right) \times \sin\left(\sqrt{\Delta^2 + 2\lambda_1^2}t\right), \tag{C3}$$

indicating that interdot triplet pairing occurs exclusively when both couplings $\lambda_{1,2} \neq 0$. For vanishing Γ_N, the relaxation mechanism is blocked, hence under such conditions, $C_{12}^{\mathrm{T}}(t)$ acquires oscillatory behavior with a convolution of the frequency $\sqrt{2}\lambda_2$ and $\sqrt{2}\lambda_1(1 + \Delta^2/2\lambda_1^2)^{1/2}$.

More general results obtained numerically for finite Γ_N are presented in Figs. 17 and 18. Again we notice that the triplet nonlocal pairing survives only temporarily, in similar fashion as the singlet nonlocal pairing does. Magnetic field affects the profile of quantum oscillations, however, in contrast with the singlet interdot pairing, it seems that $C_{12}^{\mathrm{T}}(t)$ survives over pretty long timescale upon increasing B_z (Fig. 17). Apparently, this is related to the coexistence of magnetism and triplet pairing [86]. Hybridization of boundary modes ε_M is another factor that prolongs the existence of nonlocal triplet pairing (Fig. 18). Such an effect is perhaps less surprising because the degree of overlapping Majorana modes goes hand in hand with the shortening of the topological nanowire, which can be expected to favor the mutual interdot pairing.

[1] A. Yu. Kitaev, Unpaired Majorana fermions in quantum wires, Phys. Usp. **44**, 131 (2001).

[2] N. Read and D. Green, Paired states of fermions in two dimensions with breaking of parity and time-reversal symmetries and the fractional quantum Hall effect, Phys. Rev. B **61**, 10267 (2000).

[3] M. A. Silaev and G. E. Volovik, Andreev-Majorana bound states in superfluids, J. Exp. Theor. Phys. **119**, 1042 (2014).

[4] R. Aguado, Majorana quasiparticles in condensed matter, Riv. Nuovo Cimento **40**, 523 (2017).

[5] M. Sato and A. Yoichi, Topological superconductors: a review, Rep. Prog. Phys. **80**, 076501 (2017).

[6] R. M. Lutchyn, E. P. A. M. Bakkers, L. P. Kouwenhoven, P. Krogstrup, C. M. Marcus, and Y. Oreg, Majorana zero modes in superconductor–semiconductor heterostructures, Nat. Rev. Mater. **3**, 52 (2018).

[7] E. Prada, P. San-Jose, M. W. A. de Moor, A. Geresdi, E. J. H. Lee, J. Klinovaja, D. Loss, J. Nygård, R. Aguado, and L. P. Kouwenhoven, From Andreev to Majorana bound states in hybrid superconductor-semiconductor nanowires, Nat. Rev. Phys. **2**, 575 (2020).

[8] K. Flensberg, F. von Oppen, and A. Stern, Engineered platforms for topological superconductivity and Majorana zero modes, Nat. Rev. Mater. **6**, 944 (2021).

[9] A. Yazdani, F. von Oppen, B. I. Halperin, and A. Yacoby, Hunting for Majoranas, Science **380**, eade0850 (2023).

[10] D. Aasen, M. Hell, R. V. Mishmash, A. Higginbotham, J. Danon, M. Leijnse, T. S. Jespersen, J. A. Folk, C. M. Marcus, K. Flensberg, and J. Alicea, Milestones toward Majorana-based quantum computing, Phys. Rev. X **6**, 031016 (2016).

[11] T. Dvir, G. Wang, N. van Loo, C. X. Liu, G. P. Mazur, A. Bordin, S. L. D. Ten Haaf, J. Y. Wang, D. van Driel, F. Zatelli, X. Li, F. K. Malinowski, S. Gazibegovic, G. Badawy, E. P. A.M. Bakkers, M. Wimmer, and L. P. Kouwenhoven, Realization of a minimal Kitaev chain in coupled quantum dots, Nature (London) **614**, 445 (2023).

[12] A. Bordin, C.-X. Liu, T. Dvir, F. Zatelli, S. L. D. ten Haaf, D. van Driel, G. Wang, N. van Loo, T. van Caekenberghe, J. C. Wolff, Y. Zhang, G. Badawy, S. Gazibegovic, E. P. A. M. Bakkers, M. Wimmer, L. P. Kouwenhoven, and G. P. Mazur, Signatures of Majorana protection in a three-site Kitaev chain, arXiv:2402.19382.

[13] S. Tewari, C. Zhang, S. Das Sarma, C. Nayak, and D.-H. Lee, Testable signatures of quantum nonlocality in a two-dimensional chiral p-wave superconductor, Phys. Rev. Lett. **100**, 027001 (2008).

[14] L. Fu, Electron teleportation via Majorana bound states in a mesoscopic superconductor, Phys. Rev. Lett. **104**, 056402 (2010).

[15] X.-Q. Li and L. Xu, Nonlocality of Majorana zero modes and teleportation: Self-consistent treatment based on the Bogoliubov–de Gennes equation, Phys. Rev. B **101**, 205401 (2020).

[16] Y. Hao, G. Zhang, D. Liu, and D. E. Liu, Anomalous universal conductance as a hallmark of non-locality in a Majorana-hosted superconducting island, Nat. Commun. **13**, 6699 (2022).

[17] D. E. Liu, M. Cheng, and R. M. Lutchyn, Probing Majorana physics in quantum-dot shot-noise experiments, Phys. Rev. B **91**, 081405(R) (2015).

[18] C. W. J. Beenakker and D. O. Oriekhov, Shot noise distinguishes Majorana fermions from vortices injected in the edge mode of a chiral p-wave superconductor, SciPost Phys. **9**, 080 (2020).

[19] V. Perrin, M. Civelli, and P. Simon, Identifying Majorana bound states by tunneling shot-noise tomography, Phys. Rev. B **104**, L121406 (2021).

[20] S. Smirnov, Majorana differential shot noise and its universal thermoelectric crossover, Phys. Rev. B **107**, 155416 (2023).

[21] M. Leijnse and K. Flensberg, Scheme to measure Majorana fermion lifetimes using a quantum dot, Phys. Rev. B **84**, 140501(R) (2011).

[22] D. E. Liu and H. U. Baranger, Detecting a Majorana-fermion zero mode using a quantum dot, Phys. Rev. B **84**, 201308(R) (2011).

[23] M. Lee, J. S. Lim, and R. López, Kondo effect in a quantum dot side-coupled to a topological superconductor, Phys. Rev. B **87**, 241402(R) (2013).

[24] M. Cheng, M. Becker, B. Bauer, and R. M. Lutchyn, Interplay between Kondo and Majorana interactions in quantum dots, Phys. Rev. X **4**, 031051 (2014).

[25] E. Vernek, P. H. Penteado, A. C. Seridonio, and J. C. Egues, Subtle leakage of a Majorana mode into a quantum dot, Phys. Rev. B **89**, 165314 (2014).

[26] M. T. Deng, S. Vaitiekenas, E. B. Hansen, J. Danon, M. Leijnse, K. Flensberg, J. Nygård, P. Krogstrup, and C. M. Marcus,

Majorana bound state in a coupled quantum-dot hybrid-nanowire system, Science **354**, 1557 (2016).
[27] David A. Ruiz-Tijerina, E. Vernek, Luis G. G. V. Dias da Silva, and J. C. Egues, Interaction effects on a Majorana zero mode leaking into a quantum dot, Phys. Rev. B **91**, 115435 (2015).
[28] E. Prada, R. Aguado, and P. San-Jose, Measuring Majorana nonlocality and spin structure with a quantum dot, Phys. Rev. B **96**, 085418 (2017).
[29] S. Hoffman, D. Chevallier, D. Loss, and J. Klinovaja, Spin-dependent coupling between quantum dots and topological quantum wires, Phys. Rev. B **96**, 045440 (2017).
[30] A. Ptok, A. Kobiałka, and T. Domański, Controlling the bound states in a quantum-dot hybrid nanowire, Phys. Rev. B **96**, 195430 (2017).
[31] I. Weymann and K. P. Wójcik, Transport properties of a hybrid Majorana wire-quantum dot system with ferromagnetic contacts, Phys. Rev. B **95**, 155427 (2017).
[32] M.-T. Deng, S. Vaitiekėnas, E. Prada, P. San-Jose, J. Nygård, P. Krogstrup, R. Aguado, and C. M. Marcus, Nonlocality of Majorana modes in hybrid nanowires, Phys. Rev. B **98**, 085125 (2018).
[33] J. F. Silva, L. G. G. V. Dias da Silva, and E. Vernek, Robustness of the Kondo effect in a quantum dot coupled to Majorana zero modes, Phys. Rev. B **101**, 075428 (2020).
[34] J. E. Sanches, L. S. Ricco, Y. Marques, W. N. Mizobata, M. de Souza, I. A. Shelykh, and A. C. Seridonio, Majorana molecules and their spectral fingerprints, Phys. Rev. B **102**, 075128 (2020).
[35] P. Majek and I. Weymann, Majorana mode leaking into a spin-charge entangled double quantum dot, Phys. Rev. B **104**, 085416 (2021).
[36] P. Majek, G. Górski, T. Domański, and I. Weymann, Hallmarks of Majorana mode leaking into a hybrid double quantum dot, Phys. Rev. B **106**, 155123 (2022).
[37] G. S. Diniz and E. Vernek, Majorana correlations in quantum impurities coupled to a topological wire, Phys. Rev. B **107**, 045121 (2023).
[38] L. Baldo, L. G. G. V. Dias Da Silva, A. M. Black-Schaffer, and J. Cayao, Zero-frequency supercurrent susceptibility signatures of trivial and topological zero-energy states in nanowire junctions, Supercond. Sci. Technol. **36**, 034003 (2023).
[39] R. Tuovinen, Electron correlation effect in superconducting nanowires in and out of equilibrium, New J. Phys. **23**, 083024 (2021).
[40] R. Tuovinen, E. Perfetto, R. van Leeuwen, G. Stefanucci, and M. A. Sentef, Distinguishing Majorana zero modes from impurity states through time-resolved transport, New J. Phys. **21**, 103038 (2019).
[41] B. Pandey, N. Mohanta, and E. Dagotto, Out-of-equilibrium Majorana zero modes in interacting Kitaev chains, Phys. Rev. B **107**, L060304 (2023).
[42] B. Bauer, T. Karzig, R. V. Mishmash, A. E. Antipov, and J. Alicea, Dynamics of Majorana-based qubits operated with an array of tunable gates, SciPost Phys. **5**, 004 (2018).
[43] J. Barański, M. Barańska, T. Zienkiewicz, R. Taranko, and T. Domański, Dynamical leakage of Majorana mode into side-attached quantum dot, Phys. Rev. B **103**, 235416 (2021).
[44] I. J. van Beek, A. Levy Yeyati, and B. Braunecker, Nonequilibrium charge dynamics in Majorana-Josephson devices, Phys. Rev. B **98**, 224502 (2018).
[45] P. Dutta, J. Cayao, A. M. Black-Schaffer, and P. Burset, Nonlocality of Majorana bound states revealed by electron waiting times in a topological Andreev interferometer, Phys. Rev. Res. **6**, L012062 (2024).
[46] A. Oguri, Y. Tanaka, and A. C. Hewson, Quantum phase transition in a minimal model for the Kondo effect in a Josephson junction, J. Phys. Soc. Jpn. **73**, 2494 (2004).
[47] J. Liu, J. Wang, and F.-C. Zhang, Controllable nonlocal transport of Majorana fermions with the aid of two quantum dots, Phys. Rev. B **90**, 035307 (2014).
[48] K. Wrześniewski, B. Baran, R. Taranko, T. Domański, and I. Weymann, Quench dynamics of a correlated quantum dot sandwiched between normal-metal and superconducting leads, Phys. Rev. B **103**, 155420 (2021).
[49] R. Taranko and T. Domański, Buildup and transient oscillations of Andreev quasiparticles, Phys. Rev. B **98**, 075420 (2018).
[50] N. Bondyopadhaya and D. Roy, Dynamics of hybrid junctions of Majorana wires, Phys. Rev. B **99**, 214514 (2019).
[51] W. Feng, L. Qin, and X.-Q. Li, Cross correlation mediated by Majorana island with finite charging energy, New J. Phys. **23**, 123032 (2021).
[52] T. Zienkiewicz, J. Barański, G. Górski, and T. Domański, Leakage of Majorana mode into correlated quantum dot nearby its singlet-doublet crossover, J. Phys.: Condens. Matter **32**, 025302 (2020).
[53] G. Górski, J. Barański, I. Weymann, and T. Domański, Interplay between correlations and Majorana mode in proximitized quantum dot, Sci. Rep. **8**, 15717 (2018).
[54] J. Barański, A. Kobiałka, and T. Domański, Spin-sensitive interference due to Majorana state on the interface between normal and superconducting leads, J. Phys.: Condens. Matter **29**, 075603 (2017).
[55] J. Bauer, A. Oguri, and A. C. Hewson, Spectral properties of locally correlated electrons in a Bardeen-Cooper-Schrieffer superconductor, J. Phys.: Condens. Matter **19**, 486211 (2007).
[56] A. Martín-Rodero and A. Levy Yeyati, Josephson and Andreev transport through quantum dots, Adv. Phys. **60**, 899 (2011).
[57] R. Seoane Souto, A. E. Feiguin, A. Martín-Rodero, and A. Levy Yeyati, Transient dynamics of a magnetic impurity coupled to superconducting electrodes: Exact numerics versus perturbation theory, Phys. Rev. B **104**, 214506 (2021).
[58] J. Bedow, E. Mascot, and D. K. Morr, Emergence and manipulation of non-equilibrium Yu-Shiba-Rusinov states, Commun. Phys. **5**, 281 (2022).
[59] K. Wrześniewski, I. Weymann, N. Sedlmayr, and T. Domański, Dynamical quantum phase transitions in a mesoscopic superconducting system, Phys. Rev. B **105**, 094514 (2022).
[60] L. C. Ortmanns, J. Splettstoesser, and M. R. Wegewijs, Transient transport spectroscopy of an interacting quantum dot proximized by a superconductor: Charge and heat currents after a switch, Phys. Rev. B **108**, 085426 (2023).
[61] K. G. Wilson, The renormalization group: Critical phenomena and the Kondo problem, Rev. Mod. Phys. **47**, 773 (1975).
[62] R. Bulla, T. A. Costi, and T. Pruschke, Numerical renormalization group method for quantum impurity systems, Rev. Mod. Phys. **80**, 395 (2008).
[63] Ö. Legeza, C. P. Moca, A. I. Tóth, I. Weymann, and G. Zaránd, Manual for the flexible DM-NRG code, arXiv:0809.3143 (the

open access Flexible DM-NRG Budapest code is available at http://www.phy.bme.hu/~dmnrg/).

[64] T. Domański, I. Weymann, M. Barańska, and G. Górski, Constructive influence of the induced electron pairing on the Kondo state, Sci. Rep. **6**, 23336 (2016).

[65] F. B. Anders and A. Schiller, Real-time dynamics in quantum-impurity systems: A time-dependent numerical renormalization-group approach, Phys. Rev. Lett. **95**, 196801 (2005).

[66] H. T. M. Nghiem and T. A. Costi, Time-dependent numerical renormalization group method for multiple quenches: Application to general pulses and periodic driving, Phys. Rev. B **90**, 035129 (2014).

[67] K. Wrześniewski and I. Weymann, Quench dynamics of spin in quantum dots coupled to spin-polarized leads, Phys. Rev. B **100**, 035404 (2019).

[68] R. S. Souto, A. Martín-Rodero, and A. Levy Yeyati, Andreev bound states formation and quasiparticle trapping in quench dynamics revealed by time-dependent counting statistics, Phys. Rev. Lett. **117**, 267701 (2016).

[69] R. Seoane Souto, A. Martín-Rodero, and A. Levy Yeyati, Quench dynamics in superconducting nanojunctions: Metastability and dynamical Yang-Lee zeros, Phys. Rev. B **96**, 165444 (2017).

[70] C. Stahl and M. Eckstein, Electronic and fluctuation dynamics following a quench to the superconducting phase, Phys. Rev. B **103**, 035116 (2021).

[71] M. Kamp and B. Sothmann, Higgs-like amplitude dynamics in superconductor-quantum-dot hybrids, Phys. Rev. B **103**, 045414 (2021).

[72] A. de la Torre, D. M. Kennes, M. Claassen, S. Gerber, J. W. McIver, and M. A. Sentef, Colloquium: Nonthermal pathways to ultrafast control in quantum materials, Rev. Mod. Phys. **93**, 041002 (2021).

[73] J. J. He, T. K. Ng, P. A. Lee, and K. T. Law, Selective equal-spin Andreev reflections induced by Majorana fermions, Phys. Rev. Lett. **112**, 037001 (2014).

[74] H.-H. Sun, K.-W. Zhang, L.-H. Hu, C. Li, G.-Y. Wang, H.-Y. Ma, Z.-A. Xu, C.-L. Gao, D.-D. Guan, Y.-Y. Li, C. Liu, D. Qian, Y. Zhou, L. Fu, S.-C. Li, F.-C. Zhang, and J.-F. Jia, Majorana zero mode detected with spin selective Andreev reflection in the vortex of a topological superconductor, Phys. Rev. Lett. **116**, 257003 (2016).

[75] R. Seoane Souto, K. Flensberg, and M. Leijnse, Timescales for charge transfer based operations on Majorana systems, Phys. Rev. B **101**, 081407(R) (2020).

[76] E. Mascot, T. Hodge, D. Crawford, J. Bedow, D. K. Morr, and S. Rachel, Many-body Majorana braiding without an exponential Hilbert space, Phys. Rev. Lett. **131**, 176601 (2023).

[77] G. Kells, D. Meidan, and P. W. Brouwer, Near-zero-energy end states in topologically trivial spin-orbit coupled superconducting nanowires with a smooth confinement, Phys. Rev. B **86**, 100503(R) (2012).

[78] D. Roy, N. Bondyopadhaya, and S. Tewari, Topologically trivial zero-bias conductance peak in semiconductor Majorana wires from boundary effects, Phys. Rev. B **88**, 020502(R) (2013).

[79] C.-X. Liu, J. D. Sau, T. D. Stanescu, and S. Das Sarma, Andreev bound states versus Majorana bound states in quantum dot-nanowire-superconductor hybrid structures: Trivial versus topological zero-bias conductance peaks, Phys. Rev. B **96**, 075161 (2017).

[80] C. Moore, C. Zeng, T. D. Stanescu, and S. Tewari, Quantized zero-bias conductance plateau in semiconductor-superconductor heterostructures without topological Majorana zero modes, Phys. Rev. B **98**, 155314 (2018).

[81] F. Setiawan, Chun-Xiao Liu, Jay D. Sau, and S. Das Sarma, Electron temperature and tunnel coupling dependence of zero-bias and almost-zero-bias conductance peaks in Majorana nanowires, Phys. Rev. B **96**, 184520 (2017).

[82] Ching-Kai Chiu and S. Das Sarma, Fractional Josephson effect with and without Majorana zero modes, Phys. Rev. B **99**, 035312 (2019).

[83] A. Vuik, B. Nijholt, A. R. Akhmerov, and M. Wimmer, Reproducing topological properties with quasi-Majorana states, SciPost Phys. **7**, 061 (2019).

[84] C. Moore, T. D. Stanescu, and S. Tewari, Two-terminal charge tunneling: Disentangling Majorana zero modes from partially separated Andreev bound states in semiconductor-superconductor heterostructures, Phys. Rev. B **97**, 165302 (2018).

[85] C.-X. Liu, J. D. Sau, and S. Das Sarma, Distinguishing topological Majorana bound states from trivial Andreev bound states: Proposed tests through differential tunneling conductance spectroscopy, Phys. Rev. B **97**, 214502 (2018).

[86] A. I. Buzdin, Proximity effects in superconductor-ferromagnet heterostructures, Rev. Mod. Phys. **77**, 935 (2005).